Norwegian University
of Life Sciences

Master's Thesis 2018 30 ECTS
Faculty of Environmental Sciences and Natural Resource Management

Validation of a Wind Farm Wake Model Based on the Actuator Disc Concept in Complex Terrain

Ansgar Johan Ladstein
Master of Science, Renewable Energy

Acknowledgments

First of all, I would like to express my sincere gratitude towards my supervisor Arne Reidar Gravdahl. As Associate Professor at the Norwegian University of Life Sciences and CTO & Co-founder of WindSim AS, Arne R. Gravdahl has been a key factor for completion of this study. His assistance, guidance, and sharing of knowledge during the entire process is highly appreciated.

WindSim AS is also greatly acknowledged for letting me participate in a WindSim training course, giving me access to the latest version of WindSim (9.0.0) and for letting me work at their headquarters in Tønsberg.

Moreover, Nordkraft AS is kindly acknowledged for giving me access all the SCADA data from Nygaardsfjellet wind farm used in the study. Kristoffer Lie Hansen is acknowledged for providing the computer equipment required to carry out all the CFD simulations performed in this study. In addition, I would like to thank Professor Muyiwa Samuel Adaramola for proofreading parts of my thesis.

Finally, I would like to acknowledge the Norwegian University of Life Sciences, the administration, professors and fellow students which has been taking part in the completion of my master's degree during these two years.

Oslo, 07^{th} May 2018

Ansgar Johan Ladstein

Abstract

A wind turbine operating downwind of another will stand in the wake of the upstream turbine, resulting in decreased power generation and increased load fatigue. In order to keep wake losses at a minimum, wind farm designers rely on wake models to optimize the wind farm layout. Therefore, accurate wind turbine wake aerodynamic modelling is essential for developing cost efficient modern wind farms, that consists of a large number of wind turbines usually congregated in compact formation.

Using large sets of SCADA data, which are, on-site measurements data from full scale wind turbines and meteorological data from a wind farm located in complex terrain in the northern part of Norway, the aim of this study was to perform a comparative analysis of the newly developed numerical wake model referred to as the actuator disc method (ACD), against the two most commonly known analytical wake models namely the Jensen- and Larsen model. The simulations were performed in the state of the art Computational Fluid Dynamics (CFD) software, WindSim, which solves the Reynolds Averaged Navier-Stokes (RANS) equations for wind farm development purposes.

Results of this study showed that the ACD and Larsen wake model outperformed the Jensen model for most single wake cases. For multiple wake cases, the ACD method was found to provide the most accurate results, by capturing wake-wake and wake-terrain effect. All three wake models overestimated the wake losses for the uncalibrated results in both single and multiple wake cases. However, Due to the poor quality in measurement data discovered during this study, no clear-cut conclusion can be drawn on to which wake model performed best. The main conclusion drawn in this study emphasises the necessity of high quality measurement data for wake model validation purposes.

Keyword: Wind power, Onshore wind farm, Complex terrain, Analytical wake model, Numerical wake model, Actuator disc method (ACD), Computational fluid dynamics (CFD), WindSim.

Table of Contents

List of figures

List of tables

1 Introduction

1.1 Wind energy outlook

As of October 2017, 30 wind power projects were built in Norway. In addition, 12 projects are under construction. During 2017 four wind farms were put into operation with a total installed capacity of 324 MW. The development in 2017 is thus the largest ever seen in Norwegian wind power. As of March 2018, the total installed capacity in Norway sums up to 1190 MW. Wind power development in Norway for 2018 is expected to increase even further. The Norwegian Water Resources and Energy Directorate (NVE) and the Ministry of Petroleum and Energy (OED) have granted licenses for approximately 7400 MW wind power, corresponding to an expected production around 26 TWh. Wind farm projects with a total installed power of approximately 1650 MW are currently under construction (Weir & Aksnes 2018).

Europe installed 16.8 GW of additional wind power capacity in 2017, marking a record year on annual installations. Onshore wind power contributed with 12,484 MW new added power, 3,154 MW for the offshore sector. WindEurope's Central Scenario for 2020 provides a realistic estimate of the installed capacity in Europe for the next four years. The central scenario expects wind energy in Europe to reach 204 GW by 2020, with an average annual market of 12.6 GW (Ngheim et al. 2017). Although the offshore wind sector is showing a tendency of annual growth, onshore wind power still represents more than three-quarter of the installed capacity. Making onshore wind power by far the largest contributor to new renewable energy production.

With more than 50 GW of new additions in the 2017-2020 period under the central scenario, Europe will represent slightly less than a quarter of global installations. China expects to install 84 GW representing 38% of the total global wind power installation. Although Europe increasingly implements offshore wind power, the onshore sector stands undisputed in China, US and India accounting for well over 90% of the total expected installed capacity in 2020 as presented in Figure 1.1. Whilst uncertainty for the wind power market after 2020 is very high as most EU member states still do not have post-energy-plans in place, WindEurope's analysis of the potential conditions determining wind energy deployment post-2020 provides several potential scenarios. According to the central scenario, 323 GW of cumulative wind energy

capacity would be installed in the EU by 2030. Onshore and offshore wind sector accounting for 253 GW and 70 GW respectively (Ngheim et al. 2017).

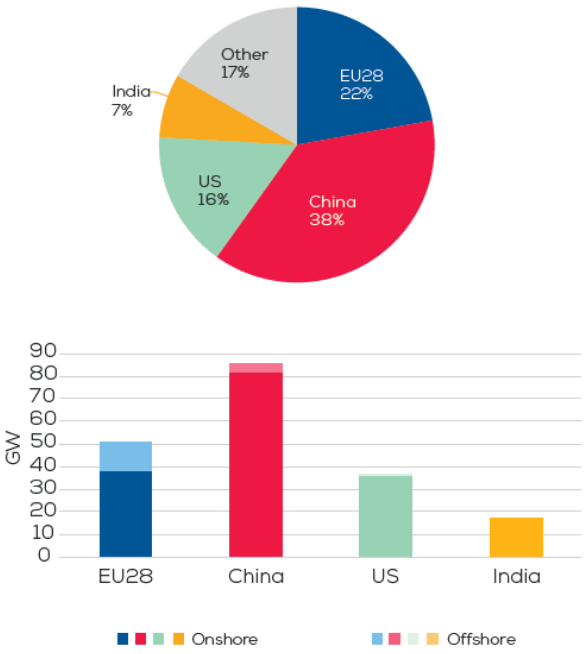

Figure 1.1 Global wind installations in 2017-2020.

The Global Wind Energy Council (GWEC) present's in the 6^{th} edition of the Global Wind Energy Outlook scenarios looking at the long-term future of the wind industry, primarily out to 2020, 2030 and forecasting to 2050. The International Energy Agency's (IEA) New Policies Scenario (NPS) is based on assessment of both national and international climate policy, commitment by governments i.e. G-8/G-20 and the Clean Energy Ministerial and various commitments to renewable energy and efficiency at national and regional level (IEA 2017). The NPS scenario project an increase to near 50 GW annually in the middle of next decade, gradually decreasing to a net of 43 GW annually by 2030. Thereafter, expecting an annual growth in the mid-30s in terms of GWs installed, remaining flat for the rest of the period out to 2050 in net terms. Consequently, cumulative installed capacity would reach 639 GW by 2020, and 1,260 GW by 2030. By 2050, NPS foresees global wind installations reaching 2,870 GW. The GWEC's moderate scenario (MS) resemble the NPS, considering all policy measures to support renewable energy either already enacted or in the planning stages on both national and international level. As well as assuming the implementation of the Paris agreement e.g. commitments for emissions reduction and keeping a global temperature rise this century well below two degrees Celsius. Moreover, MS takes into account existing and planned national and regional targets for wind energy development, the cost of wind energy continues to come down and governments beginning to respond to essential asks of national energy security and long-term price stability offered by wind energy. The results predict annual market size reaching 80 GW annually by 2020 for a total installed capacity of 797 GW. Furthermore, expecting robust growth in the period after 2020. By 2030 total installed capacity would reach nearly 1,676 GW. By 2050, MS foresees global wind power reaching 3,984 GW (Sawyer et al. 2016).

1.2 The wake effect

The rotor of the wind turbine extract energy from the wind. This leads to a deceleration of the flow downstream of the wind turbine while the turbulence in the flow increases. As the air crosses the rotor, a sudden pressure drop occurs. In the region immediately downstream of the rotor, there are non-uniform deficits of pressure and axial velocity, which are associated with the axial thrust and to the torque of the turbine (Crespo et al. 1999). The region showing a wind speed deficit and an increased turbulence intensity is called the wake of the wind turbine.

The flow field behind the turbine is characterized by strong wind shear, a high degree of turbulence and low wind speed (Magnusson & Smedman 1999). It is observed that the point of maximum velocity deficit is below the turbine axis due to the tower shadow, and the point of maximum turbulence intensity is above it. This is attributed to the shear velocity (Sanderse 2009).

Several other factors define the size and evolution of the wake structure such as wake added turbulence, geographical characteristics, turbine specifications e.g. the thrust coefficient of the turbine and the structure of the boundary-layer which is greatly depended on the thermal stratification (Rados et al. 2009) (Bechmann 2006) (Edokpa & Weli 2017).

The atmospheric boundary layer is the part of the atmosphere, which is in direct contact with the surface of the earth. Most transport processes, e.g. of momentum and heat happen in this layer. During day-time, inland, with an upward heat flux from the ground, surface heating initiates large thermal motions which cause the stratification to be unstable. At night, the cooling of the surface results in the suppression of the turbulent scales. The stratification is said to be stable. Under strong winds or time intervals at which point, thermal exchange is absent, turbulence is mechanically generated by the wind gradient. The stratification becomes neutral. Stability influences the structure of turbulence. Due to cooling and heating of the air, turbulent scales experience strong diurnal variations (Bechmann 2006). Since wind turbines operate in the lowest part of the atmospheric boundary layer, calculation of the flow around them over complex terrain is severely complicated (Sanderse 2009). Atmospheric turbulence is developed as a function of surface roughness, atmospheric stability and distance above the ground (Barthelmie et al. 2015).

The rotating wake of the horizontal axis wind turbine is usually divided into two separate regions: near wake and far wake (Hashemi-Tari et al. 2014). As the air move downstream, the cylindrical shear layer expands, due to the difference in velocity between the air inside and

outside the wake (Sanderse 2009). The pressure increases and the velocity inside the wake decrease until ambient pressure is reached. As the length of the expansion region reaches about one rotor diameter, turbulent diffusion of momentum becomes the main mechanism. The end of the near-wake region is reached at about two to five turbine diameters after the turbulence diffusion causes the shear layer thickness to increase until it reaches the wake axis (Crespo et al. 1999). The near wake flow field is influenced by the rotor angular velocity and the geometry of the blade (Hashemi-Tari et al. 2014).

As the air flow proceed further downstream in a cylindrical expanding manner, the flow enters the far wake region. In the far wake, the velocity deficit gradually decays downstream of the turbine, and the wake is fully developed. Consequently, axis-symmetry and thus a self-similar wake structure can be assumed (Chacón et al. 1996). The two main mechanism determining flow conditions in the far wake are convection i.e. heat transfer due to bulk movement of air molecules and turbulent diffusion (Vermeer et al. 2003).

1.3 Objective and scope

For large-scale exploitation of wind energy, wind turbines are put together in clusters or windfarm, as a result of geographical restriction, meteorological dependencies, and foremost economic constraints. The grouping of turbines in such farms introduces two major issues: a wind turbine operating downstream of another will stand in the wake of headwind turbines, consequently producing less power. Moreover, the increased turbulence intensity shortens the lifetime of the rotors (Cleijne 1993). It has been shown that wind turbine wakes may account for a decrease on average of 10 % to 20 % of the annual power production of large wind farms in complex terrain and offshore, resulting in a considerable benefit in improving wake and wind farm modelling (Barthelmie et al. 2014).

The tendency towards ever growing windfarms introduces the necessity of accurate wind flow modelling of wind turbine wakes for layout optimization purposes. Furthermore, the impact of wind turbine wakes are of critical importance to the wind energy industry because they directly impact both the power output and the turbulence level that determines the turbine lifetime.

Flow in complex terrain displays different characteristics compared to flow over flat and homogeneous terrain e.g. offshore wind farms. This is caused by local distortion effects, which affects both the flow field and the local turbulence. Moreover, turbine positions located in

complex terrain are distributed in irregular patterns with different hub height. The flow is, therefore, more difficult to predict than flow over flat terrain since the local distortion effects are highly site dependent (Lange et al. 2017). Installing wind turbines in complex terrain increases the degree of complexity further due to wake effects, and the power production is difficult to correlate to single point wind speed measurements. More research is needed to improve the existing wind farm prediction models for use in complex terrain, and such improvements require validation through field measurements (Hansen et al. 2016).

Approaches in estimating the wake losses go from simple theoretical or empirical laws to full rotor aerodynamic calculations. The aim of this research is to compare the results of the new actuator disc method i.e. numerical wake model based on CFD, originally described by Crasto et al. (2012) and further developed and implemented by developed by Simisiroglou et al. (2017), against the two most commonly known analytical wake models i.e. the Larsen and Jensen wake model and to evaluate the methods against real measurement data from a wind farm located in complex terrain. The study is partially a continuation of the work performed by Seim et al. (2017), where three kinematic wake models were validated against the same site and production data at Nygaardsfjellet. This study will emphasize the implementation of the new Actuator Disc Method (ACD) for a specific selection of wake cases. Firstly, on single wake cases, secondly, on multiple wake cases. Using a wind farm located in complex terrain, this study will evaluate the performance accuracy of wake-terrain effects as well as wake-wake interaction present in the multiple wake cases.

2 Analytical wake models

2.1 The Jensen wake model

The Jensen (1983) wake model is one of the most commonly used among engineering applications due to its simplicity, practicality and robustness. The model presented here is a further developed wake model by Katic (1986). It is based on the description of a single wake in terms of an initial velocity deficit, and a wake decay coefficient. Distinct characteristic differs the Jensen model from most similar wake models. By letting the wind velocity inside the wake be constant, the wake velocity profile is described in a very idealized way. Actual characteristics of the turbine can be incorporated in the model and average yearly output of a wind farm can be estimated if a sufficiently map of the area around the wind farm is available and if the frequency distribution of the wind in eight direction sectors is known. The model assumes the wake behind the turbine to spread linearly as a function of downwind distance.

Here the normalized wind velocity deficit, $\delta V = \frac{U_\infty - V}{U_\infty}$, at distance x behind a single wind turbine with a thrust coefficient C_T is found by

$$\delta V = \frac{1-\sqrt{1-C_T}}{\left(1+\frac{2kx}{D}\right)^2} \tag{2.1}$$

Where k is the wake expansion coefficient, D the rotor diameter of the wind turbine and V the wind velocity in the wake at position x.

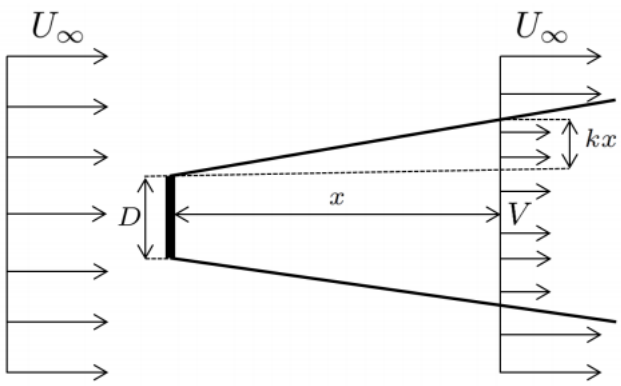

Figure 2.1 The Jensen wake model (Simisiroglou et al. 2018).

D is the rotor diameter, U_∞ the undisturbed wind velocity, x the downstream distance of the wake from the rotor, V the velocity within the wake and k the wake expansion coefficient.

One of the subcomponents of wake modelling is the wake superposition concept. In order to include the effects of all upstream turbine to the total wind deficit i.e. in multiple wake cases, 4 different approaches are mainly used. These are, geometric sum, linear sum, energy balance and quadratic sum (Göçmen et al. 2016).

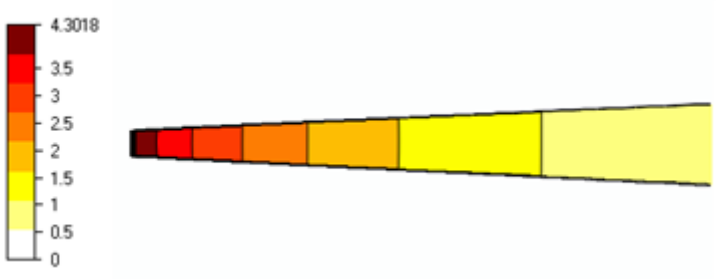

Figure 2.2 Schematic representation of the Jensen wake model (model 1) expansion of one single wind turbine on flat terrain in WindSim.

2.2 The Larsen wake model

The Larsen model is based on turbulent boundary equations and a similarity assumption. By neglecting different terms in the governing equations, two different versions of the model are presented in (Larsen 1988). The wake expands in a non-uniform manner, by differing radially in the cross-section of the wake due to the dependency of the radial distance r_x.

Here we will be using the first order wake model in which the normalized velocity deficit is given by the equation

$$\delta \mathrm{V} = \frac{\left(C_T {A_x}^{-2}\right)^{\frac{1}{3}}}{9}\left[{r_x}^{\frac{3}{2}}\left(3{c_1}^2 C_T A_x\right)^{-\frac{1}{2}} - \frac{35^{\frac{3}{10}}}{2\pi}\left(3{c_1}^2\right)^{-\frac{1}{5}}\right]^2 \tag{2.2}$$

Were r_x is the radial distance at a position x downstream of the rotor and C_T is a constant, A is the swept area of the turbine and c_1 is the Prandtl mixing length.

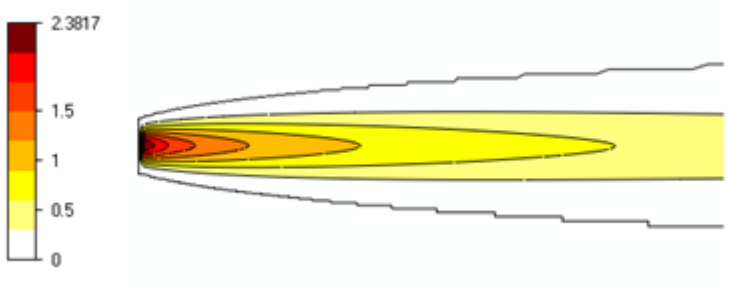

Figure 2.3 Schematic representation of the Larsen wake model (model 2) expansion of one single wind turbine on flat terrain in WindSim.

The multiple wake model implemented into WindSim for the analytical models and used in this study is based on the sum of squares. When multiple wakes influence the velocity at a position, the total normalized velocity deficit V_{tot}., is found by

$$\delta V_{tot.} = \sqrt{\sum \delta\, V_j^2} \tag{2.3}$$

Where δV_j is the normalised wind velocity deficit from the j-th wind turbine.

3 Numerical wake model based on CFD

Computational Fluid Dynamics (CFD) with the increase of computational resources has become a typical way to model wind turbines as well as wind turbine wakes. Although CFD has numerous advantages e.g. control over inflow conditions, whole flow field data of relevant parameters and other, CFD results are sensitive to the knowledge and experience of the CFD code user and to numerous computational parameters involved in the computation (Simisiroglou, N. et al. 2016). The following section presents the ACD method based on CFD and the theory behind.

3.1 One dimensional (1D) momentum theory

The base for the actuator disc method (ACD) developed and implemented in the CFD code PHOENICS (Spalding 1981), is based on the simple model of the one dimensional (1D) momentum theory first presented in the work of Rankine (1865) developed for marine propellers. A development came in the form of Froud's blade element momentum theory (1878). Betz (1921) provided an approximate correction to momentum "Rankine-Froude actuator disk" theory to account for the sudden rotation imparted to the flow by the actuator disc. Furthermore, including the maximum possible efficiency of a ground rotor or wind turbine. It may be used to estimate the thrust of an ideal wind turbine on the flow, the effects of the wind on the flow and the power of an ideal wind turbine (Simisiroglou, N. et al. 2016).

This linear momentum theory in which the wind turbine is modelled, consist of an actuator disc, i.e. with an infinite number of blades. The flow before and after the actuator disc is considered to be steady, incompressible, homogeneous, isotropic, asymmetric with constant pressure profile, non-turbulent, inviscid and neutrally stable. No rotation of the stream due to the action of the wind turbine torque is considered. Also, the thrust is assumed to be uniformly distributed over the disc area, and the velocity through the disc is considered to be constant (Göçmen et al. 2016).

Assuming a steady flow and a control volume as shown in Figure 3.1, the conservation of mass $\oint_{CV} \rho \mathbf{U} \cdot d\mathbf{A}$ dictates that the mass flow rate, $\dot{m}$, is then equal at every cross section in the control volume

$$\dot{m} = (\rho AU)_0 = (\rho AU)_D = (\rho AU)_3 \tag{3.1}$$

Where A is the area of the cross-section, ρ the density of the air, and U velocities.

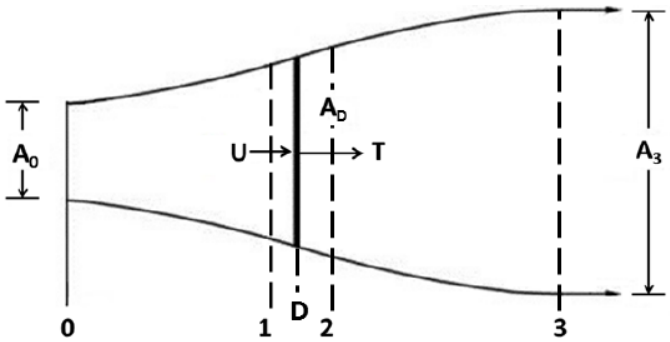

Figure 3.1 One dimensional (1 D) momentum theory.

By considering conservation of linear momentum, the thrust T applied on to the wind turbine is equal to the opposite of the change of momentum, and is given as:

$$T = U_0(\rho AU)_0 - U_3(\rho AU)_3. \tag{3.2}$$

By introducing the axial induction factor

$$a = \frac{U_0 - U_1}{U_1}, \tag{3.3}$$

and by applying Bernoulli's equation in the region before and after the disc separately, with the assumption that the axial velocity is constant when passing through the disc ($U_1 = U_2$) and that the pressure far upstream is equal to the pressure far downstream ($P_0 = P_3$), the expression for the wind turbine thrust and power extraction can be found.

$$T = \frac{1}{2}\rho A_D U_0^2 4a(1-a), \tag{3.4}$$

$$P = \frac{1}{2}\rho A_D U_0^3 4a(1-a)^2. \tag{3.5}$$

With the introduction of the thrust and power coefficients, the maximum possible efficiency of a ground rotor or wind turbine is given by

$$C_T = \frac{T}{\frac{1}{2}\rho U_0^2 A_D} = 4a(1-a). \tag{3.6}$$

$$C_P = \frac{P}{\frac{1}{2}\rho U_0^2 A_D} = 4a(1-a)^2. \tag{3.7}$$

The maximum obtainable power extraction from the flow is presented as the Betz limit. The maximum power coefficient C_{Pmax}, thus is

$$C_{Pmax} = {}^{16}/_{27} \quad \text{with} \quad a = \frac{1}{3}. \tag{3.8}$$

3.2 Actuator disc method (ACD)

The actuator disc method (ACD) is a way to represent the wind turbine's effect on the wind flow in a simulation. For the ACD method presented in Simisiroglou et al. (2017b) the thrust force T at each cell of the disc is calculated from

$$T = C_T(U_{1,i})\frac{1}{2}\rho\left(\frac{U_{1,i}}{1-\alpha_i}\right)^2 A_i \tag{3.9}$$

Where $U_{1,i}$ is the velocity of the flow at i-th cell of the disc, α_i is the axial induction factor calculated for each individual cell of the disc, A_i is the surface area of the cell facing the undisturbed wind flow direction and C_T $(U_{1,i})$ is a modified thrust coefficient dependent on the velocity at the disc $U_{1,i}$ and ρ is the air density. In most cases wind turbine manufacturers offer C_T as a function of U_∞, the undistributed wind velocity. This C_T is reasonable for the first wind turbine of the row but not for the downstream wind turbines were the flow has been disturbed. For downstream turbines, a new thrust curve which is a function of U_1 can be established from the 1D momentum theory by combining the definition of the trust coefficient C_T and the axial induction factor α

$$C_T = 4\alpha(1-\alpha) \tag{3.10}$$

$$U_1 = (1-\alpha)U_\infty \tag{3.11}$$

Hence from Eq. 3.10 and Eq. 3.11 the following is obtained

$$U_1 = U_\infty \left[1 - \frac{1}{2}\left(1 - \sqrt{1 - C_T(U_\infty)}\right)\right] \tag{3.12}$$

The power production is estimated by finding the average induction factor over the disc as $\bar{a} = \sum a_i$, and then for each velocity $U_{1.i}$ over the disc an undisturbed wind velocity $U_{\infty,i}$ is found using the following equation:

$$U_{\infty,i} = \frac{U_{1,i}}{1-\bar{a}} \tag{3.13}$$

For each undisturbed wind velocity, a power is found using the power curve and then they are averaged over the disc. Figure 3.2 shows a representation of the wake expansion of the ACD model of one single turbine operating on flat terrain and in free stream conditions.

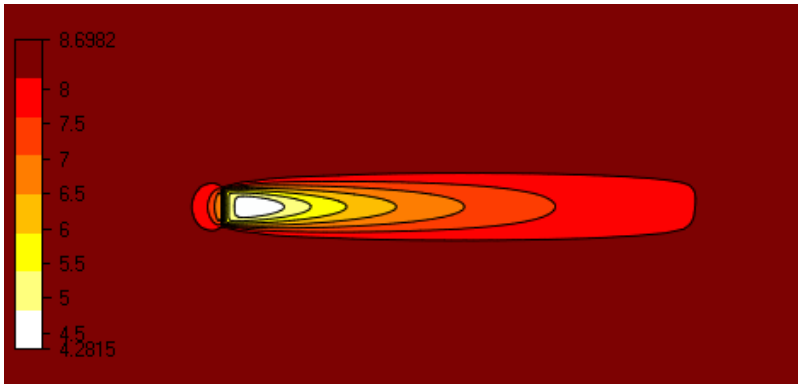

Figure 3.2 Schematic representation of wind deficit of the ACD model on flat terrain in WindSim.

3.3 Implementation of the new Actuator disc method (ACD)

In previous work from Crasto et al. (2012), an ACD method is introduced for modelling wake effects in the wind farm development software (WindSim 2018), herein referred as the old ACD method. More recently, Simisiroglou, N. et al. (2016) developed a new ACD method, herein referred as the new ACD method. The newly developed ACD method was validated against three different wind tunnel test cases.

The main differences between the new ACD model and the old method, is that the latter utilizes a uniform thrust distribution instead of calculating the thrust at each cell. Moreover, the power production of the wind turbine is assessed solely from U_1 at hub height instead of the entire rotor. Allowing the computational demands to stay at a reasonable level, providing a more user-friendly model for industrial users.

4 Materials and methodology

4.1 Wind farm site description

Nygaardsfjellet wind farm is located in the northern part of Norway (68°30'N 17°52'E) right south of E10 on Skitdalshøgda, which is about 30 km north-east of Narvik. The wind farm consists of 14 wind turbines of type Siemens SWT-2.3-93. The wind farm was established in two stages. The first three turbines (T1, T2 and T3) were put into operation in 2006, while stage two occurred in 2011 when the remaining 11 turbines were installed. Each turbine has an installed capacity of 2.3 MW and hence, the wind farm have total installed capacity of 32.2 MW. All turbines have a hub height of 80 m and rotor diameter (D) of 93 m. Average annual production of the wind farm is estimated to 105 GWh, equivalent to annual electricity consumption of about 5200 Norwegian households. The wind farm layout is shown in Figure 4.1.

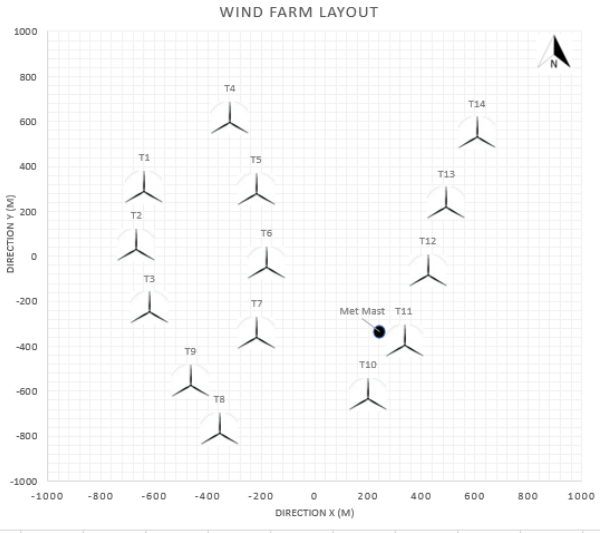

Figure 4.1 Wind farm layout.

The turbines are located in complex terrain situated between 380 m and 420 m above sea level and within an area of about 1.5 km2. Two lakes, which are Lake Nedre and Øvre Jernvatnet, partially surrounds the farm in the south, and Lake Skitdalsvatnet is located inside the wind farm. They are oriented in the north-south direction and can be described as three nonparallel rows (as can be seen in Figure 4.2), with eastward "in-row" distances of more than 3D between the turbines. The distances between the turbines in the west-east direction varies from approximately 4.5D to 10D.

Figure 4.2 Wind farm map (hoydedata.no).

Wind measurements recorded from the met mast at the site shows strong, but steady winds with an annual mean wind speed of 6,5 m/s at the height of 40 m. The prevailing wind direction at the site is from East, as seen in Figure 4.3, accounting for over 50 % of the total wind frequency distribution. However, there is also wind flow from the west direction present at the site which contributes for about 30 % of the frequency distribution. A seasonal pattern exists with winds from the east direction, which is more frequent during the winter season and vice versa. In addition, wind speeds are higher during the winter season than in summer season. Furthermore, few periods of extreme wind speed are observed at this site. The turbine specifications and power curve are presented in Table 4.1 and Figure 4.4 respectively.

Table 4.1 Turbine specifications of operating turbines at Nygaardsfjellet.

Manufacturer	Siemens
Product name	SWT-2.3-93
Blade diameter	93 m
Hub height	80 m
Nominal Power	2.300 kW
Cut-in wind speed	4 m/s
Nominal power at	13-14 m/s
Cut-out wind speed at	25 m/s

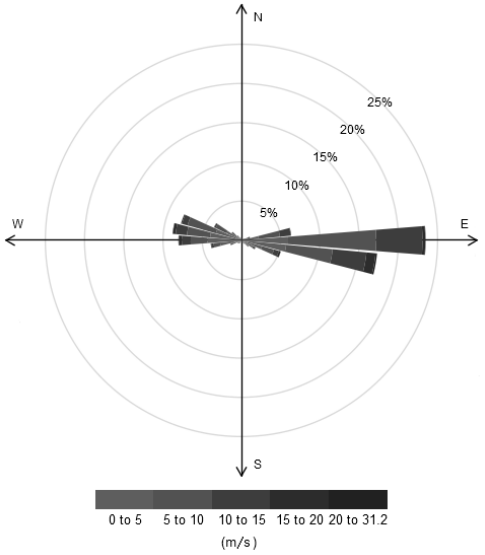

Figure 4.3 Wind rose with ten-degree bins from the met mast for the entire year.

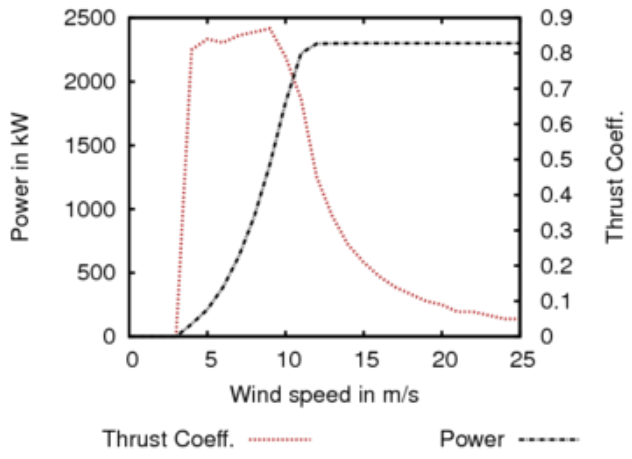

Figure 4.4 Power curve of turbine Siemens SWT-2.3-93 operating under undisturbed conditions.

4.2 Raw data sorting & filtering

One-year SCADA data, from 1 January to 31 December 2013, are collected from the Nygaardsfjellet wind farm and, used in this analysis. The data comprises production data from all the fourteen turbines and the meteorological mast, each data set containing 10 min-average data. Data recordings from each turbine include wind direction, wind speed from the two anemometers positioned on the turbine hub height and blade pitch, ambient temperature, yaw position, air density and power production. Records from the meteorological mast give information regarding wind direction, wind speed, and temperature. The wind speed is recorded for three different heights (20m, 30 m, and 40m), whereas the direction is recorded at 20 m and 40 m.

All the datasets contain some periods with no recordings, possibly due to errors with the SCADA recording system. In order to produce credible results, which are not influenced by recording errors and icy conditions, all dataset went through a filtering process. In an earlier study performed by Seim et al. (2017) at Nygaardsfjellet, these data sets were filtered using Windographer software to remove the invalid data points. Each turbine data went through several filtering processes. All recordings with power production < 0 was removed which are associated with data points where the turbine is at standstill. Furthermore, manual removal of data points that deviate largely from the power curve was performed. Meteorological data was filtered by removing data points where the anemometer recorded less than 0.4 m/s (NULL-value) for four consecutive recordings. It should be mentioned, that due to a problem with the anemometers at both 20 m and 30 m in the meteorological mast, only wind data recorded at 40 m was used in the present work.

4.3 Wake influence study

In selection of wind turbine wake cases, a significant complication in retrieving non- affected meteorological data occur due to the location of the met mast. The met mast is located within the wind farm, causing the recorded data to be wake influenced by surrounding turbines. Based on the wind farm layout (see Figure 4.1) it is highly likely that the met mast is wake influenced by turbine 11 (T11) for easterly winds. Similarly, for westerly wind condition, wake influence caused by turbine 7 (T7) is plausible.

In order to select wake cases with highest quality of the measurement data i.e. minimal wake influence, a wake influence study is performed. Using the kinematic wake model presented by

Larsen (1988), implemented in the CFD software WindSim, wake expansion is modelled. Initial conditions and settings of the simulations are presented in Table 4.2. The analytical wake model was selected for this sub-study based on it's the simplicity of use and low computational demands.

Table 4.2 Simulation parameters and initial conditions for the wake influence study.

Original grid resolution	40 x 40 km
Total number of cells	1 496 040
Sector run	24
Convergence criteria	0.005
Number of iterations sector 90° (E)	367
Number of iterations sector 270° (W)	368
Height of boundary layer height	500 m
Air density	1.225 kg/m3
Turbulence model	Standard K-epsilon
CFD solver	GCV

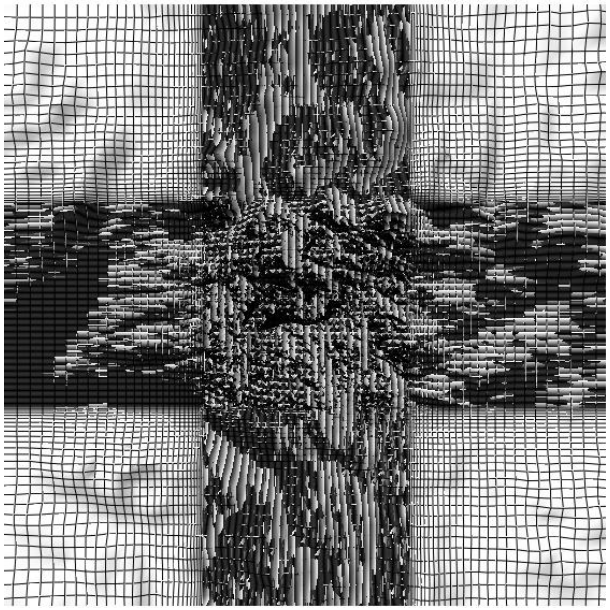

Figure 4.5 Horizontal grid showing the refinement area.

Figure 4.5 display the grid resolution at ground level of the actual grid. Body fitted coordinates (BFC) are used in the grid generation. The refinement allows for a greater accuracy in computation over the wind farm area.

Results from the simulations show that wake cases with easterly winds would lead to non-credible results. The wake created by T11 positioned less than one rotor diameter (1D) upwind from the met mast, expand directly into the met mast location. As can be observed from Figure 4.6 the met mast, represented as a grey cone, is located in the epicenter of the wake expansion of T11. The region of maximum wake influence results in a wind speed deficit of 1.58 m/s.

The simulation results for westerly winds (270 degrees), shows that wake influence on the met mast is significantly reduced compared to easterly winds, as shown in Figure 4.7. A wind deficit of 0.7 m/s at met mast location is estimated. Moreover, for North-West wind direction (280 degrees or more), wake influence is nearly absent. Based on this knowledge, exclusively wake cases with westerly winds is selected for this study. A schematic representation of the wake expansion of the Larsen and Jensen model for inflow wind direction of 285° is available in Appendix A.

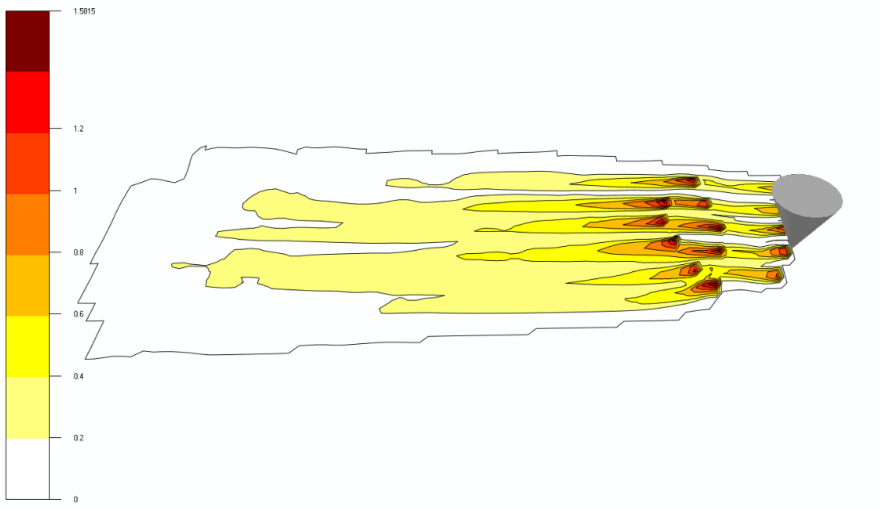

Figure 4.6 Wake development over wind farm with easterly wind direction of 90 degrees, with met mast location.

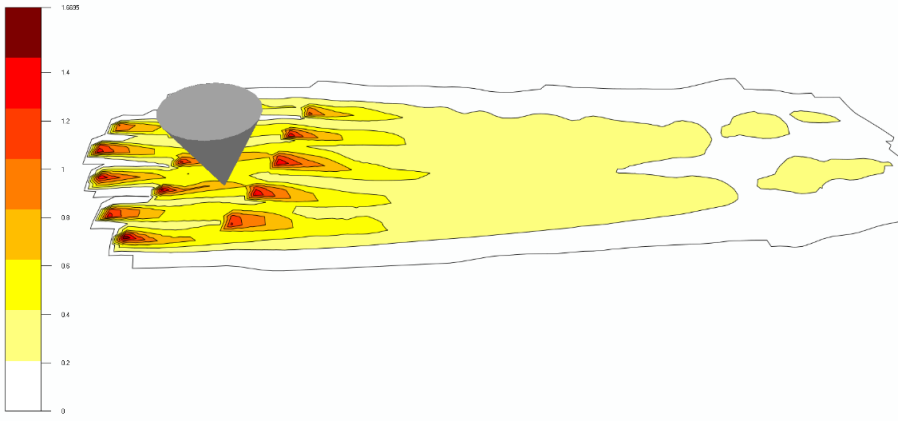

Figure 4.7 Wake development over wind farm with westerly wind direction of 270 degrees, with met mast location.

4.4 Case study set-up

As mentioned in Section 4.2, records from the wind turbines' SCADA system are available for 10 minutes periods. The power production of each wind turbine per inflow direction and undisturbed wind speed is thus available. Due to data availability limitations, the power production data are binned based on inflow directions and wind velocity measurements. The directional bins are ±2.5° wide and the velocity bins are ±0.5 m/s wide.

Based on the quantity of the SCADA measurement and wind farm layout the wake cases selected for this study are presented as follow:

(i) Five pairs of wind turbines aligned in eastward direction are used for single wake cases, with turbine 4 (T4), turbine 1 (T1), turbine 2 (T2), turbine 3 (T3) and turbine 9 (T9) operate in free stream wind conditions and are referred as the upwind turbine in each respective single wake cases. Turbine 14 (T14), turbine 5 (T5), turbine 6 (T6), turbine 7 (T7) and turbine 10 (T10) are the turbines operating in wake influenced conditions, characterized by region experiencing wind speed deficit and increased turbulence caused by the upwind turbine in each respective case. Figure 4.8 and Table 4.3 show the inflow angle for each single wake cases.

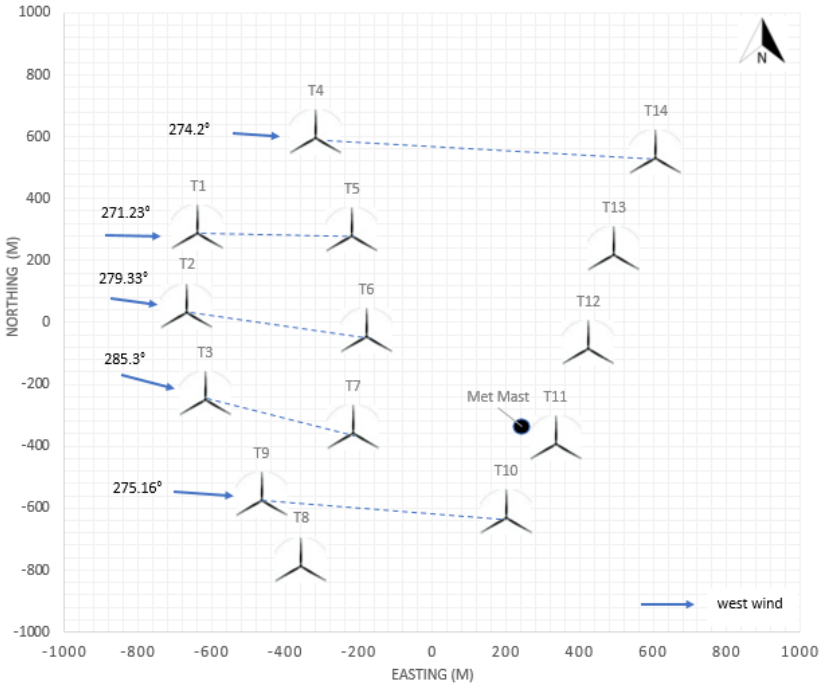

Figure 4.8 Single wake cases and inflow directions.

Table 4.3 Single wake cases with inflow wind speed above boundary layer height.

	Upwind turbine	Turbine in wake	Inflow direction	Inflow wind speed
Case #1	T4	T14	274.2°	10 m/s
Case #2	T1	T5	271.23°	10 m/s
Case #3	T2	T6	279.33°	10 m/s
Case #4	T3	T7	285.3°	10 m/s
Case #5	T9	T10	275.16°	10 m/s

(ii) Two groups of three turbines, aligned in eastward direction are selected for the multiple wake case study. Turbine 1 (T1) and turbine 2 (T2) operates in free stream conditions. Turbine 5 (T5) and turbine 6 (T6) operates in the wake of T1 and T2 respectively. Turbine 13 (T13) and turbine T12 (12) operate under multiple wake conditions affected by the turbines positioned upstream as represented in Figure 4.9 and Table 4.4.

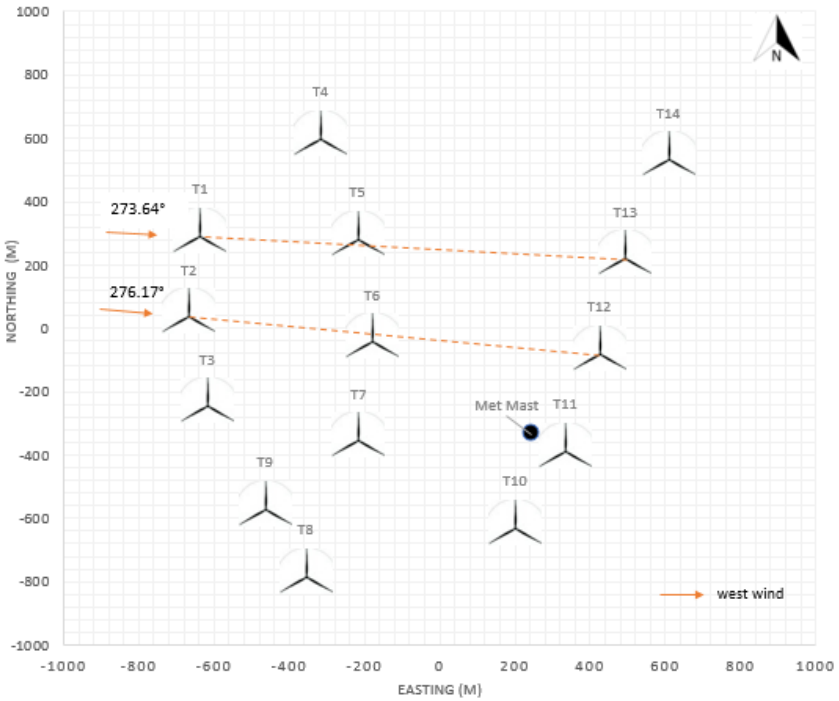

Figure 4.9 Multiple wake cases and inflow directions.

Table 4.4 Multiple wake cases with inflow wind speed above boundary layer height.

	Upwind turbine	Turbine in wake	Inflow direction	Inflow wind speed
Case #6	T1	T5, T13	273.64°	10 m/s
Case #7	T2	T6, T12	276.17°	10 m/s

4.5 Computational technique

The simulations are performed in the commercial software WindSim version 9.0.0. This software uses the general purpose CFD code PHOENICS developed by CHAM Ltd. (Concentration Heat and Momentum Limited) commercially available since 1981 (Spalding 1981) to solve the Reynolds Averaged Navier-Stokes (RANS) equations in an iterative way. To obtain the RANS equations, the unsteady turbulent flow field is averaged. This result in a set of flow equations that may have steady solutions (Wackers & Koren 2007). The flow variable solved are namely pressure, three velocity components, turbulent kinetic energy and turbulent dissipation rate. Different turbulent closures are available in WindSim and they are (i) standard $k-\varepsilon$, (ii) modified $k-\varepsilon$, (iii) $k-\varepsilon$ with YAP correction, (iv) RNG $k-\varepsilon$ and (v) the $k-\omega$ wilcox turbulence model. In this thesis, the default setting in WindSim, standard $k-\varepsilon$ turbulence model is used.

4.5.1 Digital terrain model

WindSim software is a module-based software. First, the terrain and roughness data are used as input. The original file i.e. ".gws grid file", contains data from a 40 km by 40 km area with a 20.3 m grid resolution. For each single wake cases and multiple wake cases, the grid file is rotated in an anti-clockwise manner equivalent to the angle difference between the aligned turbines and west direction i.e. 270°, as can be seen in Table 4.5. Thus, all wake cases will represent a grid with two parallel west-east aligned turbines. For example, for single wake case T4-T14 (turbine 14 in wake of turbine 4) anti-clockwise rotation of 4.2° is performed, resulting in a digital terrain model where the two turbines are aligned at the exact direction of 270°. An extension of the digital terrain model is thereafter performed in order to reduce the number of cells and the computational efforts. The model is cropped into a 10 km by 8 km grid.

Table 4.5 Grid rotation for both single and multiple wake cases.

	Inflow angle (original grid)	Grid rotation (anti-clockwise)	Inflow angle (Digital terrain model)
Single wake cases			
Case #1	274.2°	4.2°	270°
Case #2	271.23°	1.23°	270°
Case #3	279.33°	9.33°	270°
Case #4	285.3°	15.3°	270°
Case #5	275.16	5.16°	270°
Multiple wake cases			
Case #6	273.64°	3.64°	270°
Case #7	276.17°	6.17°	270°

Table 4.6 Terrain extension parameter for all wake cases for both the numerical and analytical model set-up.

	X-range (m)	Y-range (m)	Terrain extension
Single wake cases			
Case #1	17000-27000	19000-27000	10 x 8 km
Case #2	15000-25000	17000-24000	10 x 8 km
Case #3	20500-30500	22000-30000	10 x 8 km
Case #4	24000-34000	25000-33000	10 x 8 km
Case #5	17500-27500	19000-27000	10 x 8 km
Multiple wake cases			
Case #6	17000-27000	18000-26000	10 x 8 km
Case #7	18000-28000	20000-28000	10 x 8 km

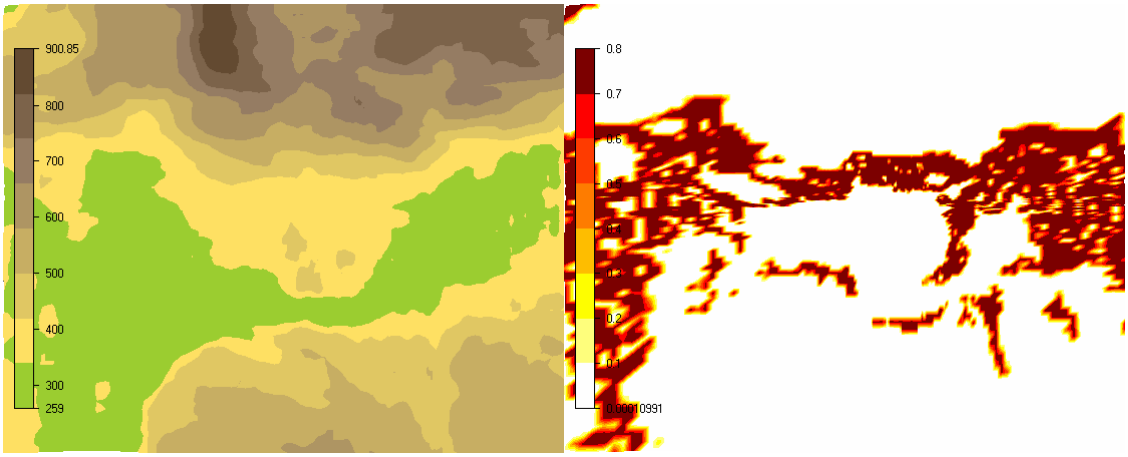

Figure 4.10 Terrain elevation (m) (left) and roughness (m) (right).

The terrain extension and range of each local grid are presented in Table 4.6 for all wake cases. The digital terrain model established for Case #1, containing elevation and roughness data for the area is given is presented in Figure 4.10 and Figure 4.11. The complexity at the site depends on the changes in elevation and roughness. Elevation complexity can be visualized by the inclination angles which is a derived quantity expressing the first order derivatives of the elevation.

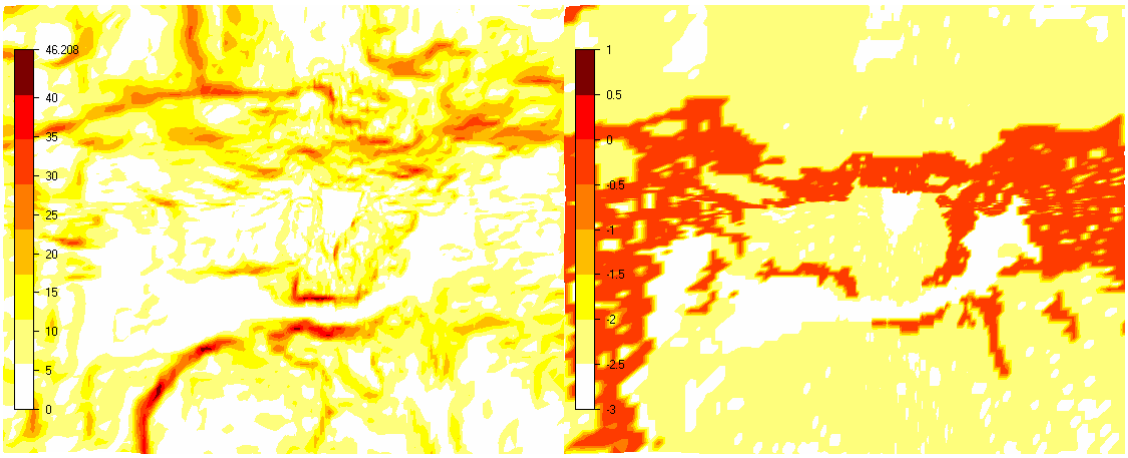

Figure 4.11 Terrain inclination (deg) (left) and logarithmic roughness (m) (right).

4.5.2 Grid independence evaluation

Dimensions of the computational domain established, is selected with basis in grid sensitivity study performed on the actuator disc by Crasto et al. (2012). A grid resolution with negligible discretization errors was achieved with a spacing of D/16^{th} (where D is the rotor diameter of the wind turbine). This is, the default setting in WindSim for the actuator disc refinement type. Moreover, the grid sensitivity study performed by Seim et al. (2017) on Nygaardsfjellet, concluded a grid independent solution achieved at 1.3 million cells. In this study, a grid independent solution is therefore assumed with high degree of confidence for simulation performed with resolution of D/16^{th} and total number of cells exceeding 1.3 million.

4.5.3 Implementation of the porous discs

By means of simple trigonometry and mathematics, new turbine coordinates corresponding to their original position was successfully retrieved for the rotated grid.

In accordance with the rule of procedure for the actuator disc, the two turbines are introduced in the module referred as the “object module” creating the porous discs i.e. “.bws blocking file”, representing the turbines. The object module holds the turbine specifications i.e. turbine coordinate, hub height, rotor diameter and the power curve introduced as the “.pws file” (Siemens_23_93SV.pws).

A refinement of the grid is defined for the domain containing the actuator discs, while outside the equidistant region the resolution expands. The terrain data is also smoothened in order to

reduce the risk of divergence in the wind field simulation. The equidistant region is automatically defined by the software after the wind turbine locations are selected. In this study grid resolution of D/16^{th} is achieved in the equidistant region in both the vertical and horizontal directions. The grid resolution at turbine position for northward and eastward direction is either 5.7 m or 5.8 m and increases with increased distance from the turbine location as shown in Table 4.7.

The refinement file created in the numerical simulation is then applied to the analytical simulation by introducing the ".bws blocking file" created for each numerical wake case simulation.

Table 4.7 Grid spacing and total number of cells of all wake cases

	Grid spacing (m)		Total number of cells
	Eastward	Northward	(grid resolution)
Single wake cases:			
Case #1	5.8 – 179.2	5.8 – 160.5	1 995 432
Case #2	5.8 - 174.1	5.7 - 163.0	1 381 955
Case #3	5.8 – 173.8	5.8 – 160.1	1 473 150
Case #4	5.8 – 181.4	5.8 – 167.3	1 381 955
Case #5	5.7 – 181.0	5.7 – 157.4	1 669 570
Multiple wake cases:			
Case #6	5.8 – 167.9	5.7 – 168.2	2 255 292
Case #7	5.7 – 180.6	5.7 – 155.9	2 280 729

Elevation and roughness data defined in the previous step is used to define the ground level of a three-dimensional domain divided into cells with a variable horizontal and vertical resolution. The grid is generated and optimized from the digital terrain model, as seen in Figure 4.12.

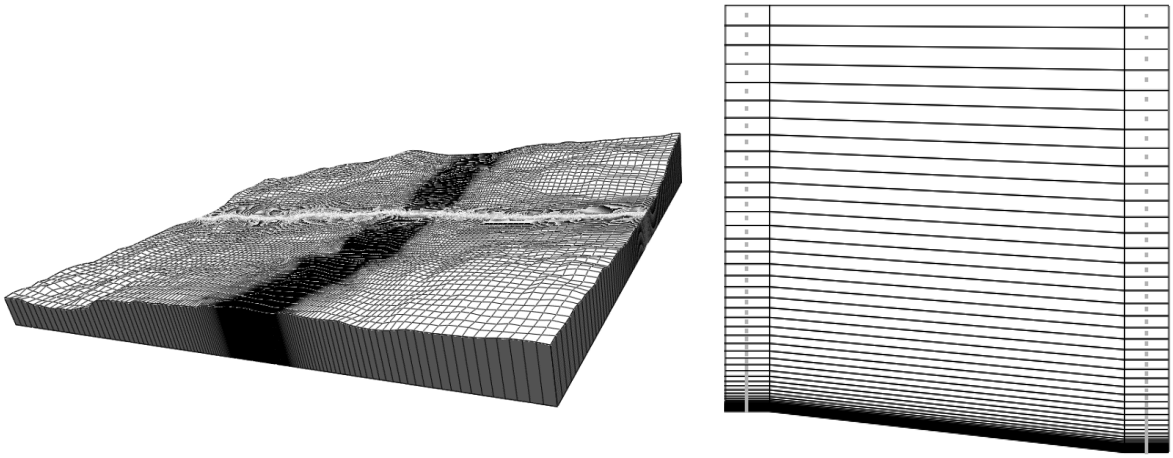

Figure 4.12 Three-dimensional grid resolution (left) and schematic view of the vertical grid resolution (right)

The grid extends 6346 m above the point in the terrain with the highest elevation. The grid is refined towards the ground. The left and right columns in Table 4.8 present the distribution at the position with maximum and minimum elevation respectively. The nodes, where results from the simulations are available, are situated in the cell centers indicated by dots.

Table 4.8 Distribution of the first 10 nodes in z-direction, relative to the ground, at the position with maximum and minimum elevation

	1	2	3	4	5	6	7	8	9	10
z-dist. max (m)	2.8	8.4	14.0	19.5	25.1	30.7	36.4	42.2	48.0	53.8
z-dist. min (m)	2.8	8.4	14.0	19.5	25.1	30.7	36.4	42.2	48.0	53.8

4.5.4 Simulations

A numerical wind database, which is used to transfer the wind conditions from the measurement point to the wind turbine hub positions, is established by CFD simulations. This section describes how the numerical model is set up, simulated and validated.

The lower representation in Figure 4.13 represents the simulation of the ACD method. Where, U_{BL} stand for wind speed above the boundary layer height and $U_{met\ mast}$ is the wind speed at met mast position at 40 m height. The numerical simulation (ACD method), uses wind speed above boundary layer as input value for wind fields calculation, contrary to the analytical model which uses $U_{met\ mast}$. Since the turbines are introduced as porous discs into the wind field calculations, wind speed deficit caused by wake effects are directly integrated into the simulations. Whereas, the analytical model only introduce the turbines after the CFD simulations. Therefore, the met mast is not influenced by the turbine's wake as shown in the upper schematic of Figure 4.13. In order to recreate the same initial

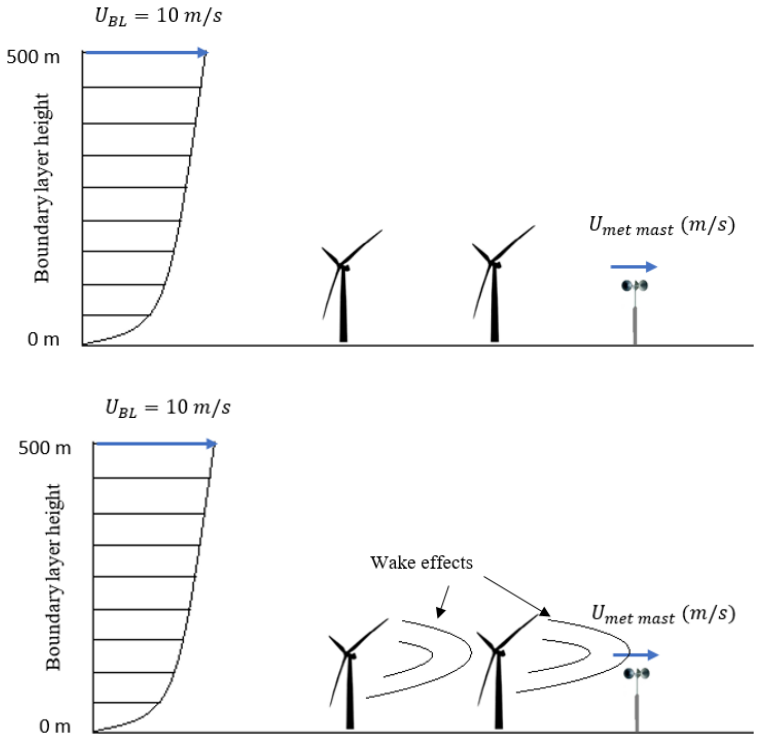

Figure 4.13 Schematic representation of the analytical simulations (over) and numerical simulations (under).

conditions between the numerical and analytical simulations, calibration of the model is necessary. Vertical profile from the met mast is extracted from the analytical model i.e. not wake influenced. By means of linear interpolation, wind speed at 40 m is calculated. The meteorological data introduced as the "climatology file" (.wws file) is adjusted to the wind speed at 40 m previously found. As a result, input value for the numerical model (U_{BL}) is equal to the input value of the analytical model ($U_{met\ mast}$). For all single (Case #1, #2, #3, #4 and #5) and multiple wake cases (Case #6 and #7), calibration of the models is performed. The simulations are therefore executed in following order

(i) The numerical model is run for all wake cases.

(ii) Wind speed at met mast location at 40 m height is extracted and implemented in the analytical model for all wake cases.

(iii) The analytical model is run for all wake cases.

The power production for the numerical model is manually extracted from the WindSim code. Power production for the analytical model is calculated in the "energy" module.

Table 4.9 wind speed value at met mast locations for input value 10 m/s above boundary layer height.

	Wind speed at met mast location, 40 m height
Single wake cases	
Case #1	8.024 m/s
Case #2	7.566 m/s
Case #3	8.139 m/s
Case #4	7.485 m/s
Case #5	7.921 m/s
Multiple wake cases	
Case #6	8,021 m/s
Case #7	8,156 m/s

Table 4.9 shows the wind speed extracted for all wake cases in the numerical simulations at met mast location and 40 m height, using input value of 10 m/s above boundary layer height.

The convergence of the wind field simulations is evaluated by inspection of the spot and residual values for the velocity components (U1, V1, W1), the turbulent kinetic energy (KE) and its dissipation rate (EP). The convergence criteria are set as default value of 0.005. When the residual value of the iterations falls below 0.005, the solution is said to be converged and is displayed with a (C). In case of divergence, a (D) is displayed. For all wake cases, convergence criteria have been reached as shown in Table 4.10. The residual and spot values for the numerical simulations of case #1 is presented in Figure 4.14. For the remaining plot, refer to Appendix C and Appendix D.

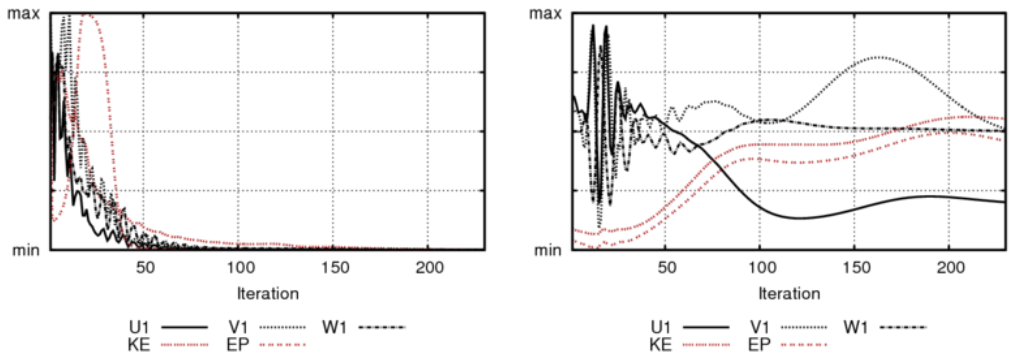

Figure 4.14 Residuals (left) and spot values (right) for the numerical simulations of case #1, sector 270.

Table 4.10 Number of iterations for sector 270 and convergence status, where C, stands for reached convergence criteria.

		Actuator disc			Analytical		
Single wake cases	sector	Simulation time	iterations	status	Simulation time	iterations	status
Case #1	270	01:43:60	230	C	01:29:40	230	C
Case #2	270	01:06:46	201	C	00:57:27	202	C
Case #3	270	01:09:02	194	C	01:01:22	195	C
Case #4	270	00:57:12	169	C	00:52:42	169	C
Case #5	270	01:22:51	202	C	01:08:42	202	C
Multiple wake cases							
Case #6	270	02:22:59	253	C	02:08:55	252	C
Case #7	270	09:27:12	236	C	02:17:58	236	C

4.5.5 Case #8

An additional case (Case #8) is performed in order to evaluate the wind speed deficit at met mast location caused by the upwind turbines. Turbines T2 and T6, which are the two turbines also operating upwind in Case #4 in addition to the original turbines T3 and T7 are implemented into the original numerical model of Case #4. The wind field simulation was restarted before extracting wind speed at met mast position as described in chapter 4.5.5. All other initial,

boundary and simulation conditions are identical to the previous cases. Case #8 showed wind speed of 7.029 m/s at 40 m at met mast location representing wind deficit of 0.456 m/s compared to single wake case #4. The schematic representation of case #8 in Figure 4.15, show how the wake-terrain and wake-wake effects affect the expansion of the wake implemented in the ACD model.

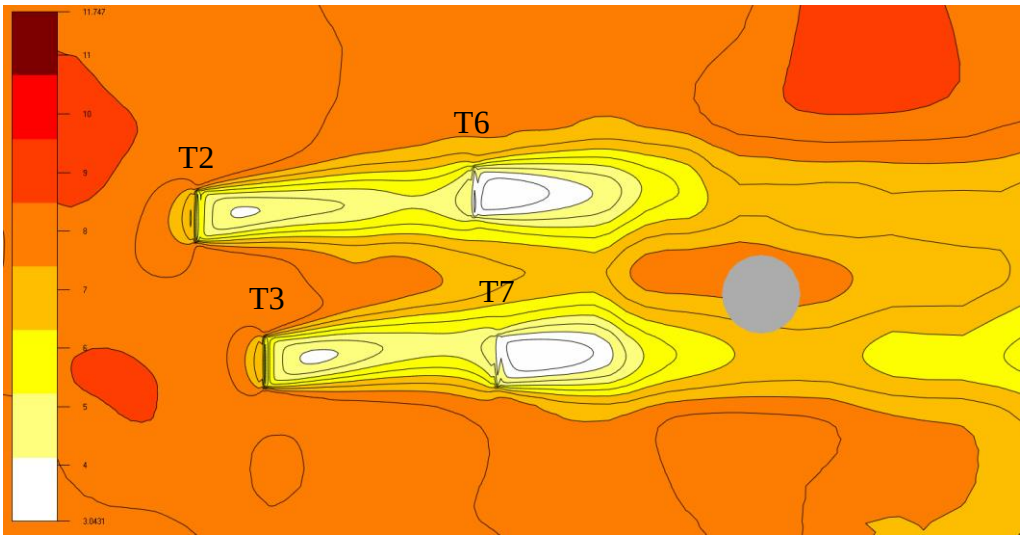

Figure 4.15 wake expansion of wake case #8 with met mast position

5 Results

Results of the comparative analysis is presented in this Chapter. Due to the non-disclosure agreement with Nordkraft Vind AS, all results are presented in normalized form. The normalization is done by dividing the power production of each wind turbine from the simulations with the measured power production of the upwind turbine of each wake cases. The reported error bar range is equal to the normalized standard deviation of the measured power production of each wind turbine. Normalized power production of all three wake models are presented with specified symbol in the figure legend, providing good visualization of the performance accuracy of the different methods.

5.1 Calibrated results

In this section, calibrated results from both single and multiple wake cases, which are wake Case #1 to Case #7 are presented, along with the calibrated performance of each wake model. The calibration is performed in order to evaluate the accuracy in predicting the wake influence performance independent of the mismatch in power production for free stream conditions (upstream turbine). Calibration is done by setting production value of the upstream turbine from the wake model, equal to the power production data of that same turbine. As the wind speed ratio upstream and downstream a wind turbine is expected to be constant for minor changes in inflow wind speeds. The wake loss percentage for the calibrated results is set equal to the wake losses originally calculated. Figure 5.1 to Figure 5.5 presents the calibrated results from the five single wake cases. Figure 5.6 and Figure 5.7 presents the calibrated results from the two multiple wake cases. Table 5.1 to Table 5.3 presents, in percentage, (i) the wake losses calculated from the production data (ii) the wake losses estimated in the analytical and numerical wake models, for the single wake cases. Table 5.4 and Table 5.5 present the wake losses for the multiple wake models.

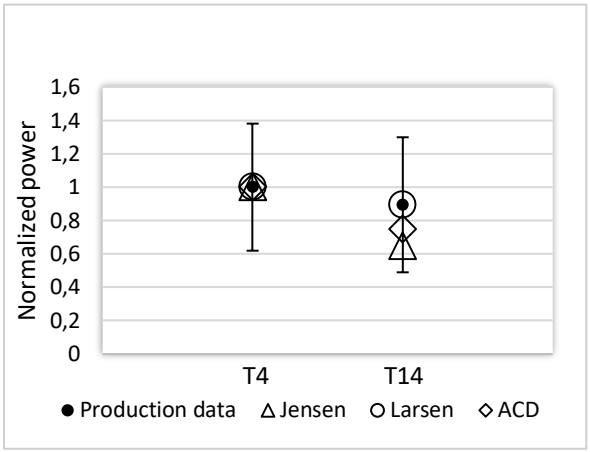

Figure 5.1 Calibrated results of single wake case #1.

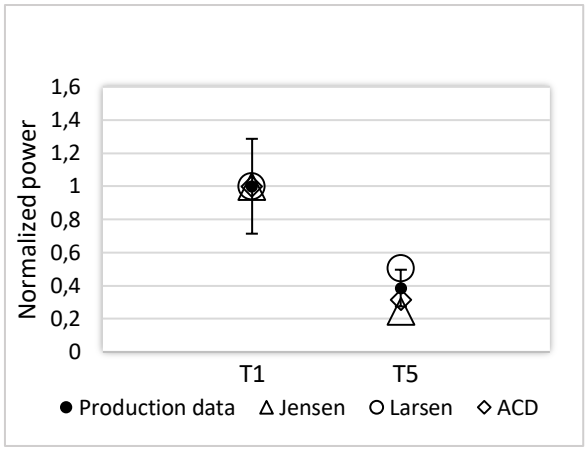

Figure 5.2 Calibrated results of single wake case #2.

Table 5.1 Wake losses values from production data and wake models for single wake case #1 (left) and single wake case #2 (right).

	Wake loss %
Production data	10.56 %
Jensen	35.19 %
Larsen	10.65 %
ACD	25.22 %

	Wake loss %
Production data	61.45 %
Jensen	75.29 %
Larsen	49.59 %
ACD	68.62 %

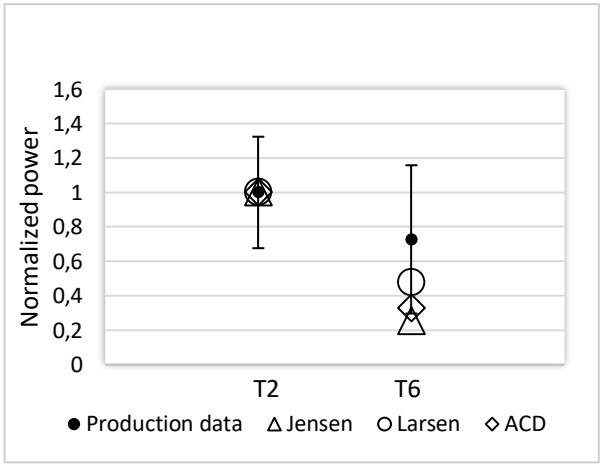

Figure 5.3 Calibrated results of single wake case #3.

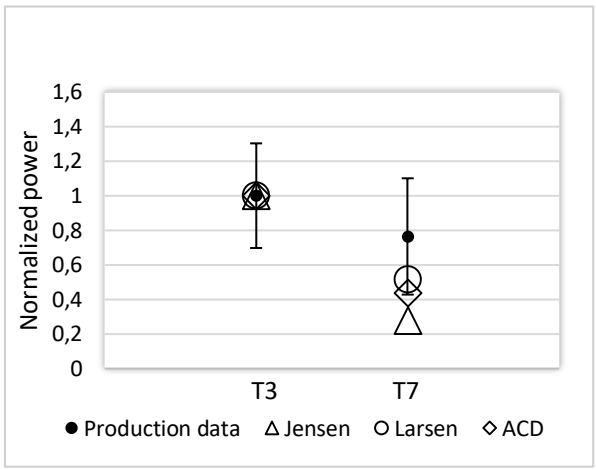

Figure 5.4 Calibrated results of single wake case #4.

Table 5.2 Wake losses values from production data and wake models for single wake case #3 (left) and single wake case #4 (right).

	Wake loss %
Production data	27.28 %
Jensen	74.54 %
Larsen	52.22 %
ACD	67.42 %

	Wake loss %
Production data	23.58 %
Jensen	72.16 %
Larsen	48.48 %
ACD	56.30 %

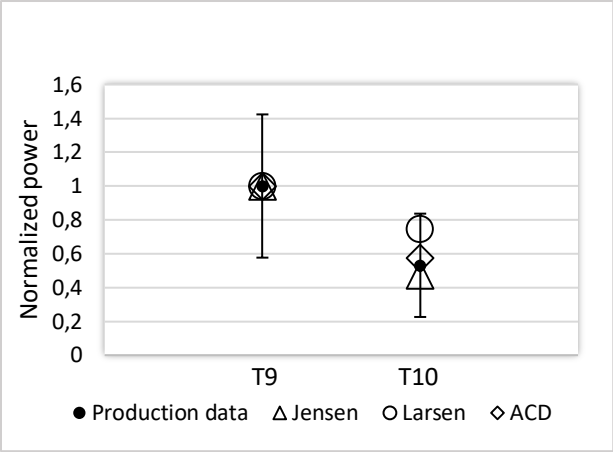

Figure 5.5 Calibrated results of single wake case #5.

Table 5.3 Wake losses values from production data and wake models for single wake case #5.

	Wake loss %
Production data	46.88 %
Jensen	52.60 %
Larsen	25.44%
ACD	42.41 %

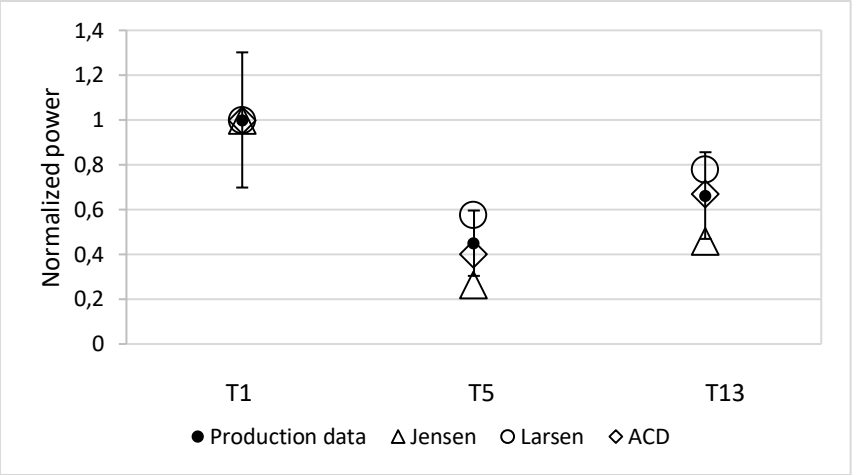

Figure 5.6 Calibrated results of multiple wake model #6.

Table 5.4 Wake losses values from production data and wake models for multiple wake case #6.

	Wake loss first turbine %	Wake loss second turbine %
Production data	55.01 %	33.74 %
Jensen	73.70 %	54.23 %
Larsen	42.41 %	22.20 %
ACD	58.89 %	32.95 %

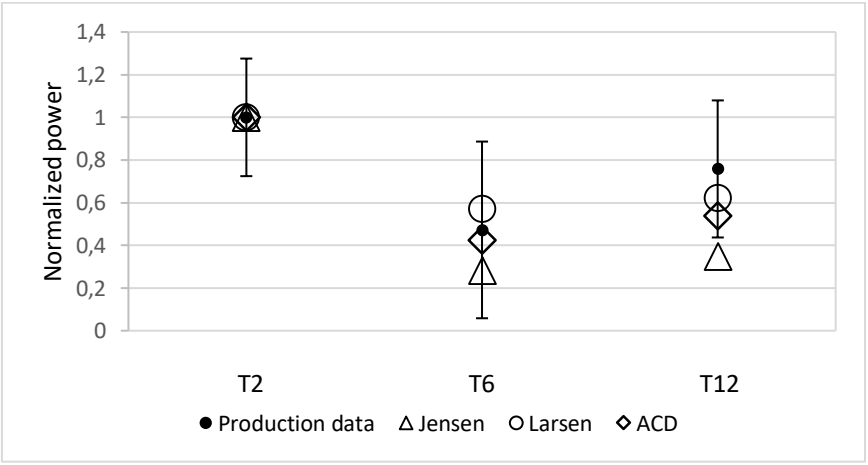

Figure 5.7 Calibrated results of multiple wake model #7.

Table 5.5 Wake losses values from production data and wake models for multiple wake case #7.

	Wake loss first turbine %	Wake loss second turbine %
Production data	52.76 %	24.18 %
Jensen	71.70 %	65.19 %
Larsen	42.87 %	37.75 %
ACD	57.48 %	46.14 %

5.2 Uncalibrated results

Figure 5.8 to Figure 5.12 presents the results from the five single wake cases. Table 5.6 to Table 5.8 presents the value of normalized power production from measurement data, the two analytical wake models and the numerical model (ACD model) for the single wakes. Normalized power production of the production data from the upstream turbine (left) is displayed as a black dot equal to 1.0 for each case. For the wake influenced turbine (right) i.e. downstream turbine, production data show decrease in the power production as expected.

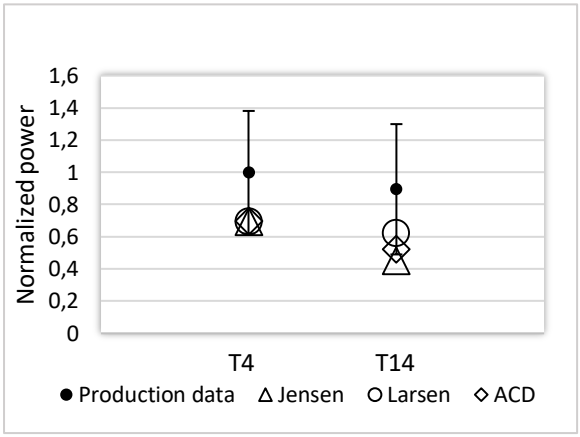

Figure 5.8 Single wake case #1.

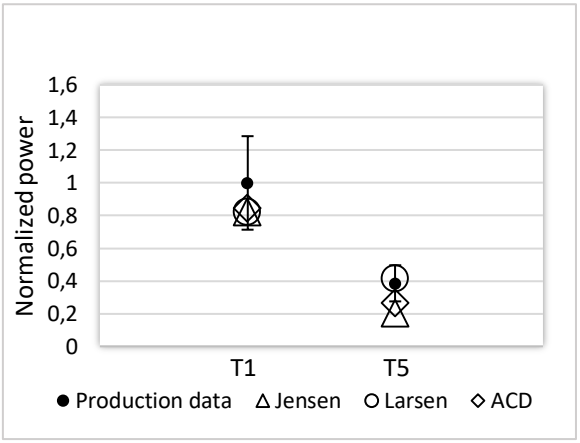

Figure 5.9 Single wake case #2.

Table 5.6 Normalized power production values for single wake case #1 (left) case #2 (right).

	Upwind Turbine	Turbine in wake
Production data	1.00	0.89
Jensen	0.69	0.45
Larsen	0.69	0.62
ACD	0.70	0.52

	Upwind Turbine	Turbine in wake
Production data	1.00	0.39
Jensen	0.82	0.20
Larsen	0.82	0.41
ACD	0.85	0.27

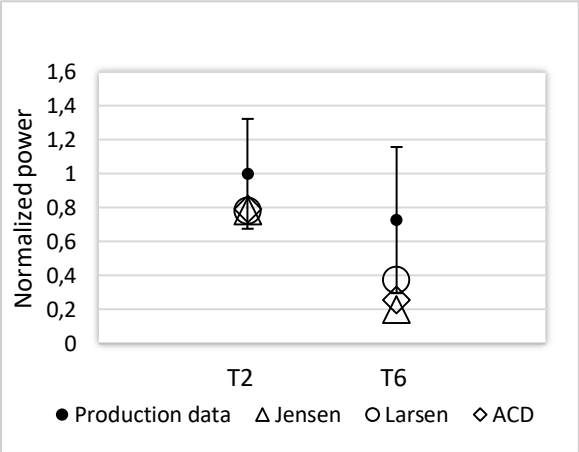

Figure 5.10 Single wake case #3.

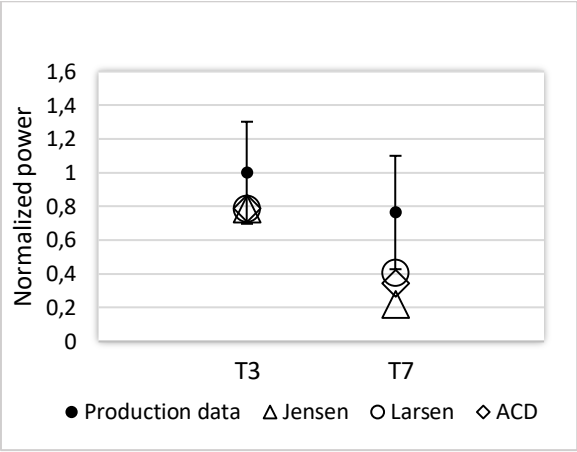

Figure 5.11 Single wake case #4.

Table 5.7 Normalized power production values for single wake case #3 (left) case #4 (right).

	Upwind Turbine	Turbine in wake
Production data	1.00	0.73
Jensen	0.78	0.20
Larsen	0.78	0.37
ACD	0.79	0.26

	Upwind Turbine	Turbine in wake
Production data	1.00	0.76
Jensen	0.79	0.22
Larsen	0.79	0.40
ACD	0.79	0.35

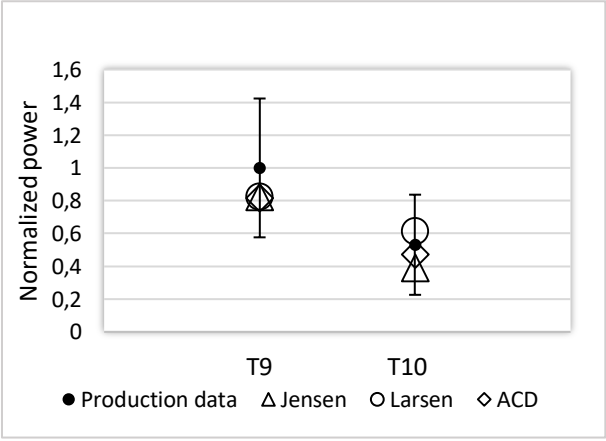

Figure 5.12 Single wake case #5.

Table 5.8 Normalized power production values for single wake case #5.

	Upwind Turbine	Turbine in wake
Production data	1.00	0.53
Jensen	0.82	0.39
Larsen	0.82	0.61
ACD	0.82	0.47

Figure 5.13 and Figure 5.14 presents the results of the two multiple wake cases. Upstream turbines are represented by T1 and T2, second turbine influenced by the single upstream turbine are T5 and T6. The third turbine, which is wake influenced by the wake interaction of the two upstream turbines are T13 and T12 for Case #6 and Case #7 respectively. Table 5.9 and Table 5.10 presents the value of normalized power production from measurement data, the two analytical wake models and the numerical model (ACD model) for the multiple wake cases.

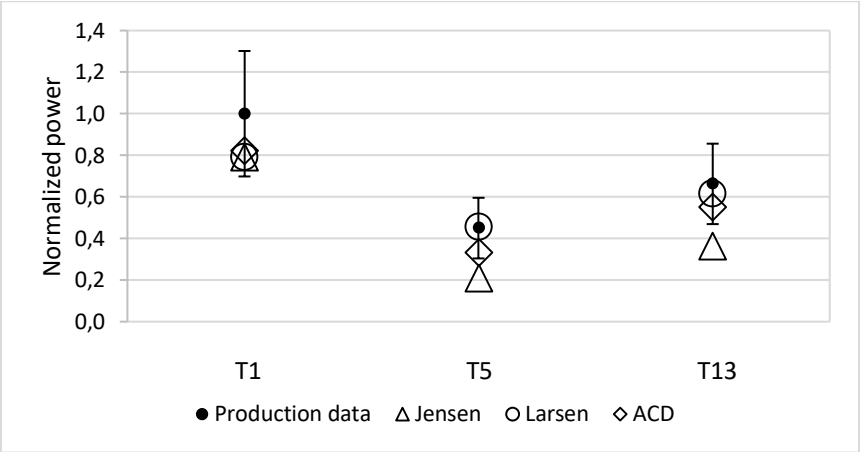

Figure 5.13 Multiple wake case #6.

Table 5.9 Normalized power production values for multiple wake case #6.

Case #1 T1 T5 T13	Upwind Turbine	Turbine in single wake	Turbine in multiple wake
Production data	1.00	0.45	0.66
Jensen	0.79	0.21	0.36
Larsen	0.79	0.45	0.61
ACD	0.82	0.33	0.55

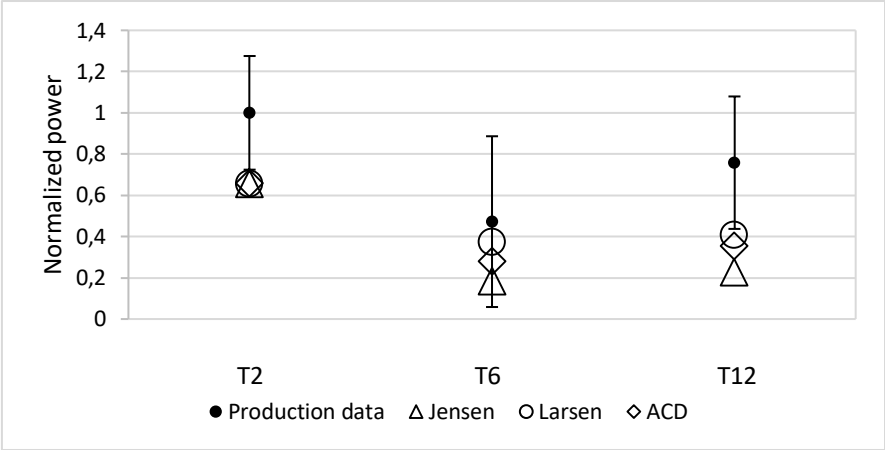

Figure 5.14 Multiple wake case #7.

Table 5.10 Normalized power values for multiple wake case #7.

Case #1 T1 T5 T13	Upwind Turbine	Turbine in single wake	Turbine in multiple wake
Production data	1.00	0.47	0.76
Jensen	0.66	0.19	0.23
Larsen	0.66	0.38	0.41
ACD	0.66	0.28	0.35

6 Discussion

The aim of this study was to provide a comprehensive analysis of analytical and numerical wake models using a large set of production data from a wind farm located in complex terrain. A set of test cases were performed to test the accuracy of the wake models and to evaluate their performance in reproducing wake-terrain and wake-wake effects. Large differences in the wake model's estimation of the energy loss in the wake was found.

From the results section presented in Chapter 5 without the correction, both the analytical and numerical wake models underestimated the power production for all single wake cases, in the range of 0.15 to 0.30 (expressed as normalized power production) for the upwind turbine operating in free stream conditions. For multiple wake cases, the models underestimated the energy production within a range of 0.18 to 0.34. The Jensen and Larsen model predicted exact same power production for all upwind turbines in both single and multiple wake cases. However, the ACD model differed minimally from the analytical models in a range of 0.1 to 0.3 for three of the single wake cases and one multiple case. The ACD modelled exact same value as the analytical models for the remaining three cases. Both the analytical and numerical wake models have previously proven to predict accurate results (Gaumond et al. 2012), especially for single turbine operating in free stream conditions. It is therefore highly unlikely that these results are caused by incorrect models and simulations. Several factors can explain the observed deviation:

(i) Wake influence on the meteorological mast:

Results from the wake influence study, support the hypothesis that measurement data recorded from the meteorological mast contains affected values caused by wake effects of surrounding turbines. The study provided good understanding of the flow fields within the windfarm enabling to select the most suitable cases. However, regarding the selected wake cases, turbine pairs with the most westerly wind direction (closest to 270°) exert highest wake influence on the meteorological mast. The higher the inflow wind direction (angle) difference from direct west, the lower the wake influence on the met mast. For single wake cases, cases with highest to lowest wake influence are expected to be as follow: Case #2 with a deviation of 1.23°, Case #1, Case #5, Case #3 and finally case #4 with a deviation of 4.72°, 5.16°, 9.33° and 15.3°

respectively. However, results from the power production deficit do not correlate with direction deviation, meaning that wake influence only partially explains the production gap between the wake models and the measurement data. Results from Case #8 performed to evaluate the wake influence on one specific case (case #4) showed a wind speed of 7.029 m/s at met mast location (40 m height), resulting in wind speed deficit of 0.456 m/s compared to the original case #4, which was simulated analytically i.e. not including wake effects.

Former validation study performed on Nygaardsfjellet support the conclusion of wake influence of the meteorological SCADA data drawn in this study. In the work of (Seim et al. 2017), high value of standard deviation from the production data with easterly wind direction correlates well with the wake influence effects. In the work of (Jiayi 2017), the analytical wake model underestimated significantly the energy production compared to the real measurement.

(ii) Quality of SCADA data:

Quality of the measurement data complicated considerably filtration and validation of the model. The aim of this study was to recreate very specific wake cases under narrow specific conditions. Therefore, high quality of the measurement data in the extracted segment is necessary. Uncertainty in the measurements, as is the nature of field data, complicated the validation due to the fact of nature which is not at steady state contrary to the simulations. Results from the single and multiple wake cases showed that cases with highest quality of SCADA data i.e. shortest range-bar representing standard deviations, provides the best prediction of power production. For single wake cases, Case #2 provided the most accurate results with a standard deviation of 0.286 m/s for upwind turbine and 0.110 m/s for the turbine in wake. For multiple wake cases, Case #6 predicted best results with standard deviation of 0.302 m/s for upwind turbine, 0.146 m/s for first turbine in wake and 0.193 m/s for second turbine. The high values of standard deviations support the conclusion of poor quality of the measurement data. The evaluated cases analyze the power production of the turbines in one single wind direction with velocity bin of 1m/s. Therefore, the interval of power production is expected to stay at a minimum. Theoretically, by using the power curve of the operating turbines at Nygaardsfjellet wind farm, the expected standard deviation can be calculated. At wind speed of 8m/s ± 0.5m/s, the power production data range within the interval of 0.83-1.217, where 1.0 is the normalized power production of 941 kW at 8m/s. Turbine 5 (T5) and turbine 13 (T3), are the only two turbines providing measurements data to fall within this range. It should be mentioned that due to selection of sector bins, production data of high quality would

still exceed these values, nonetheless minimally. Moreover, manufacturer's power curve does not realistically represent the operation parameters as they are affected by local conditions.

(iii) General issues regarding complex terrain:

Former validation studies also mentioned the difficulty in the verification of flow model in complex terrain. In the study of Barthelmie et al. (2011), several influencing factors are mentioned. These factors include difficulty due to interpretation of terrain effect, irregular location of wind turbines, short data period and poor data quality. The fact that wind farm developer at any time strive to avoid wake effects, wind turbines are positioned in such a manner that prevailing wind directions avert turbine rows. Therefore, when filtrating measurement data for two or more aligned wind turbine pairs from most wind farms, short available period of data is highly likely.

The calibrated results provide an overview of the performance accuracy between the different wake models for the wake influenced turbine in each wake cases. The actuator disc approach provided good agreement with the measurements of highest quality. For all wake cases, the Larsen model predicted the highest energy production. The second analytical wake model, Jensen model, predicted lowest energy production in all cases i.e. overestimating most the wake losses. While the numerical wake model (ACD method) predicted power production, ranging between the production of the two analytical models. The same pattern was observed for the multiple wake cases. In single wake Case #1, the Larsen model predicted the most accurately with wake loss of 10.65% compared to 10.56% for the production data. The ACD model performed best in two of the single wake cases with wake loss of 68.62% for Case # 2 and 42.41% for Case #5 compared to 61.45% and 46.88% of the production data respectively. For the last two single wake cases, all wake models underestimated the energy production, Larsen model being the least far off with wake loss prediction difference of nearly 25% for both Case #4 and Case #5. (Gaumond et al. 2012) found the Larsen model to underestimating the power deficit in single-wake cases at both Horns Rev- and Lillgrund wind farm. In the study of Duckworth & Barthelmie (2008), using measurement data from two onshore wind farms, both the Larsen- and Jensen model showed varying performance. The ACD method is more computationally demanding than the analytical simulations and is expected to treat wake-wake and wake-terrain effects with more precision. Wind tunnel tests have shown that the ACD method proves accurate results for far-wake conditions (Kalvig et al. 2012). In the implementation of the new ACD method performed by Simisiroglou et al. (2017) in wind tunnel experiment, the results showed satisfactory agreement between the simulations and the

measurements for set-up with both one single turbine and with two in-line wind turbines. Considering the simplicity and computational needs of the method. In the recent work of Simisiroglou et al. (2018) on Lillgrund wind farm, the new ACD method and Larsen model outperformed the other wake models.

The ACD method performed best in multiple wake Case #6 with wake loss of 58.89% for T5 and 32.95% for T13 compared to 55.01% and 33.74% for the production data respectively. Resulting in prediction accuracy of 93% for T5 and 98% for T13. For the last multiple wake Case #7, the ACD performed best for T6 with wake loss of 57.48% against 52.76% in measurements data. For T12, all wake model overestimated the wake losses, Larsen being the least far off with wake loss of 36.75% compared to 24.18% of the production data. Moreover, an increase in production is observed for the second turbine in wake (T12 and T13) for both multiple wake models. This phenomenon can be explained from the terrain effects as presented in Appendix D. T12 and T13 are located on the east side of lake Skitdalsvatnet creating a speed up effect right before reaching the turbines location, under westerly wind direction as used in this study. Resulting in a higher energy production compared to the turbine operating downstream of the first turbine in each case.

Looking at the distances between each turbine pairs a pattern in the wake prediction can be observed. T4 and T14 from Case #1 are the two turbines separated with the highest distance, equivalent to 9.97D, D being the rotor diameter. Correlating well with the fact that Case #1 causes the lowest wake losses on the downstream turbine. The turbines in Case #2, Case #3 and Case #4 are separated by approximately same distances (4.5D, 5.31D and 4.48D respectively). All three wake models predicted relative identical wake loss between each case. In all three cases, the Jensen model predicted wake loss of 72% to 75%, The Larsen model 48% to 52% and finally the ACD predicting wake loss of 56% to 68%. On the other hand, measurement from the production data does not provide the same picture. Wake losses in Case #2 represent over 61% against 27% and 24% for Case #3 and Case #4 respectively. From this analysis, the gap in wake losses provided by the measurement data in these three observed cases again put into question the reliability and quality of the data.

Comparing the results from the wake influence study against wake Case #8, the difference in interpreting the terrain effects between the analytical and numerical model is shown. The Larsen model used in the wake influence study disregard on a much higher level the terrain effects, causing the wake to expand independently from the ground. Whereas, the ACD method which

directly implements the turbines in the wind field simulations, enables the model to include the interactions of wake and terrain effects as shown in Figure 4.15.

It should be mentioned that several aspects has not been taking into consideration throughout this study and that the limitations set could have a significant impact on the findings. The restricting factors runs as follow:

(i) CFD simulations.

Complex terrain has always been a challenge for the wind energy industry. CFD models, plays a key role as they should be capable of accurately describing the wind field over complex terrain. The new ACD method provides an improvement regarding the computational demand decreasing the need for computer capacity. But it still needs adequate amount of data and knowledge regarding the input parameters. CFD modelling requires a lot of expertise and experience.

(ii) Manufacturer's power curve is used.

As previously mentioned the power curve at local conditions are affected by environmental conditions, e.g. air temperature, turbulence intensity or air density. In reality, the turbines operate in a range of power curves.

(iii) Directional selection of wake cases.

For single wake cases, the study only exanimates cases where the wind direction is in-line to the row of the wind turbine. For multiple wake cases, the study only examines cases where the wind direction is in-line with the first and third turbine. Resulting in a misalignment of the centered turbine.

(iv) Only the $k - \varepsilon$ turbulence model is used.

The CFD model assumes a neutral stratification of the atmosphere, a non-realistic assumption in many cases, especially in complex terrain conditions. As mentioned in the introduction it must be expected that the stratification is at stable state conditions during the winter season. Resulting in varying wake losses between the seasons.

(v) The directional uncertainty as presented by (Gaumond et al. 2013) has not been considered.

(vi) The data has not been filtered for stability.

(vii) Yaw misalignment errors are only corrected for T6.

7 Conclusions & future work

Significant differences in the prediction capabilities of the numerical and analytical wake models were found. Overall, findings showed that the ACD and Larsen model outperformed the Jensen model for most single wake cases. In some cases, all three wake models showed a tendency to overestimate the wake losses. Results presented in the work of (Seim et al. 2017), concluded likewise, the Larsen model performed better than the Jensen model at Nygaardsfjellet. The ACD model outperformed the two analytical wake models for multiple wake cases, indicating that the ACD managed to interpret wake-terrain and wake-wake effects on a higher level than the kinematic models. For the uncalibrated results, all three wake models overpredicted the wake losses. However, due to the lack of quality in the meteorological SCADA data discovered during this study, no clear-cut conclusions can be drawn on the which model performed best. Findings reveal the importance of meticulously selecting met mast locations when developing wind farms, and the impact of wake effects on the data. The study shows the necessity of high-quality data for validation purposes and the challenges involved in extracting such information. Validation studies in complex terrain should be performed using more than one measurement point. (Politis et al. 2011) emphasized the need for "multi-mast campaigns" in such terrain, enabling to capture and measure the wind shear and atmospheric stability at different heights. Over more, findings reveal the improvement in the new ACD model, regarding the computational demands and its simplicity of use.

Future work would include caring out the proposed method for wind farms, that holds sets of high-quality SCADA data. Furthermore, as stability has an impact on wake development it is important to explore wind farm cases in which the data has been filtered for stability and to evaluate the wake model's performance using different stability parameter on wind farms located in complex terrain.

In the field of wind industry and energy sector in general, the significance of this study is primarily aimed towards wind farm developers, and to which extent, decision making in implementing meteorological masts in operating wind farms could affect the course of wake model's improvements, which in turn entails in optimization of wind farm layouts and their profitability.

References

Barthelmie, R., T Frandsen, S., Rathmann, O., Hansen, K., Politis, E., Prospathopoulos, J., G Schepers, J., Rados, K., Cabezon, D., Schlez, W., et al. (2011). *Flow and wakes in large wind farms: Final report for UPWIND WP8*.

Barthelmie, R., T. Frandsen, S., Rathmann, O., Hansen, K., Politis, E., Prospathopoulos, J., Cabezon, D., Rados, K., P. van der Pijl, S., G. Schepers, J., et al. (2014). *Flow and wakes in large wind farms in complex terrain and offshore*.

Barthelmie, R. J., Churchfield, M. J., Moriarty, P. J., Lundquist, J. K., Oxley, G. S., Hahn, S. & Pryor, S. C. (2015). The role of atmospheric stability/turbulence on wakes at the Egmond aan Zee offshore wind farm. *Journal of Physics: Conference Series*, 625 (1).

Bechmann, A. (2006). *Large-Eddy Simulation of Atmospheric Flow over Complex Terrain* Risø National Laboratory Technical University of Denmark

Chacón, L., Crespo, A., Enevoldsen, P., Gómez-Elvira, R., Hernández, J., Højstrup, J., Manuel, F. & Thomsen, K. (1996). Measurements on and modelling of offshore wind farms. In Frandsen, S. T. (ed.), 87-550-2190-5.

Cleijne, J. W. (1993). Results of Sexbierum Wind Farm; single wake measurements. Apeldoorn: TNO lnstitute of Environmental and Energy Technology.

Crasto, G., Gravdahl, A. R., Castellani, F. & Piccioni, E. (2012). Wake Modeling with the Actuator Disc Concept. *Energy Procedia*, 24: 385-392. doi: https://doi.org/10.1016/j.egypro.2012.06.122.

Crespo, A., Hernández, J. & Frandsen, S. (1999). Survey of modelling methods for wind turbine wakes and wind farms. *Wind Energy*, 2 (1): 1-24.

Duckworth, A. & Barthelmie, R. J. (2008). Investigation and Validation of Wind Turbine Wake Models. *Wind Engineering*, 32 (5): 459-475. doi: 10.1260/030952408786411912.

Edokpa, D. O. & Weli, V. E. (2017). An Assessment of Atmospheric Boundary Layer Turbulence in Maiduguri, Nigeria. *Open Journal of Air Pollution*, Vol.06No.02: 17. doi: 10.4236/ojap.2017.62003.

Gaumond, M., Réthoré, P.-E., Bechmann, A., Ott, S., Larsen, G. C., Pena Diaz, A. & Hansen, K. S. (2012). *Benchmarking of Wind Turbine Wake Models in Large Offshore Windfarms*.

Gaumond, M., Réthoré, P. E., Ott, S., Peña, A., Bechmann, A. & Hansen, K. S. (2013). Evaluation of the wind direction uncertainty and its impact on wake modeling at the Horns Rev offshore wind farm. *Wind Energy*, 17 (8): 1169-1178. doi: 10.1002/we.1625.

Göçmen, T., Laan, P., Réthoré, P., Diaz, A., Larsen, G. C. & Ott, S. (2016). Wind turbine wake models developed at the technical university of Denmark: A review. *Renewable and Sustainable Energy Reviews*, 60: 752-769. doi: https://doi.org/10.1016/j.rser.2016.01.113.

Hansen, K. S., Larsen, G. C., Menke, R., Vasiljevic, N., Angelou, N., Feng, J., Zhu, W. J., Vignaroli, A., Liu, W. W., Xu, C., et al. (2016). Wind turbine wake measurement in complex terrain. *Journal of Physics: Conference Series*, 753 (3): 032013.

Hashemi-Tari, P., Siddiqui, K., Refan, M. & Hangan, H. (2014). Wind Tunnel Investigation of the Near-wake Flow Dynamics of a Horizontal Axis Wind Turbine. *Journal of Physics: Conference Series*, 524 (1): 012176.

IEA. (2017). *World Energy Outlook 2017*.

Jensen, N. O. (1983). A note on wind generator interaction, 87-550-0971-9.

Jiayi, J. (2017). *Wind Resource Assessment in Cold Climate Regions*: The Arctic University of Norway.

Kalvig, S., Manger & Hjertager. (2012). *Comparing different CFD wind turbine modelling approaches with wind tunnel measurements*, vol. 555.

Katic, I. (1986). A simple model for cluster efficiency: European Wind Energy Association Conference and Exhibition.

Lange, J., Mann, J., Berg, J., Parvu, D., Kilpatrick, R., Costache, A., Chowdhury, J., Siddiqui, K. & Hangan, H. (2017). For wind turbines in complex terrain, the devil is in the detail. *Environmental Research Letters*, 12 (9): 094020.

Larsen, C. G. (1988). A Simple Wake Calculation Procedure, 87-550-1484-4.

Magnusson, M. & Smedman, A. S. (1999). Air flow behind wind turbines. *Journal of Wind Engineering and Industrial Aerodynamics*, 80 (1): 169-189. doi: https://doi.org/10.1016/S0167-6105(98)00126-3.

Ngheim, A., Fraile, D., Mbistrova, A. & Remy, T. (2017). Wind energy in europe: Outlook to 2020. In Pineda, I. (ed.): Wind Europe.

Politis, E. S., Prospathopoulos, J., Cabezon, D., Hansen, K. S., Chaviaropoulos, P. K. & Barthelmie, R. J. (2011). Modeling wake effects in large wind farms in complex terrain: the problem, the methods and the issues. *Wind Energy*, 15 (1): 161-182. doi: 10.1002/we.481.

Rados, K. G., Prospathopoulos, J., Politis, E., Chaviaropoulos, P. K. & Zervos, A. (2009). *CFD modeling issues of wind turbine wake under stable atmospheric conditions*, vol. 6.

Sanderse, B. (2009). *Aerodynamics of wind turbine wakes Literature review*.

Sawyer, S., Teske, S., Fried, L. & Shukla, S. (2016). *Global Wind Energy Outlook 2016*.

Seim, F., Gravdahl, A. R. & Adaramola, M. S. (2017). Validation of kinematic wind turbine wake models in complex terrain using actual windfarm production data. *Energy*, 123: 742-753. doi: https://doi.org/10.1016/j.energy.2017.01.140.

Simisiroglou, N., Karatsioris, M., Nilsson, K., Breton, S. P. & Ivanell, S. (2016). The Actuator Disc Concept in Phoenics. *Energy Procedia*, 94: 269-277. doi: https://doi.org/10.1016/j.egypro.2016.09.182.

Simisiroglou, N., Sarmast, S., Breton, S. P. & Ivanell, S. (2016). Validation of the actuator disc approach in PHOENICS using small scale model wind turbines. *Journal of Physics: Conference Series*, 753 (3): 032028.

Simisiroglou, N., Breton, S. P. & Ivanell, S. (2017a). Validation of the actuator disc approach using small-scale model wind turbines. *Wind Energ. Sci.* , 2 (2): 601.

Simisiroglou, N., Philippe B, S. & Ivanell, S. (2017b). *Validation of the actuator disc approach using small scale model wind turbines*.

Simisiroglou, N., Polatidis, H. & Ivanell, S. (2018). Wind farm power production assessment: a comparative analysis of two actuator disc methods and two analytical wake models. *Wind Energ. Sci. Discuss.*, 2018: 1-13. doi: 10.5194/wes-2018-8.

Spalding, D. B. (1981). A general purpose computer program for multi-dimensional one- and two-phase flow. *Mathematics and Computers in Simulation*, 23 (3): 267-276. doi: https://doi.org/10.1016/0378-4754(81)90083-5.

Vermeer, L. J., Sørensen, J. N. & Crespo, A. (2003). Wind turbine wake aerodynamics. *Progress in Aerospace Sciences*, 39 (6): 467-510. doi: https://doi.org/10.1016/S0376-0421(03)00078-2.

Wackers, J. & Koren, B. (2007). Multigrid solution method for the steady RANS equations. *Journal of Computational Physics*, 226 (2): 1784-1807. doi: https://doi.org/10.1016/j.jcp.2007.06.007.

Weir, D. E. & Aksnes, N. (2018). Vindkraft- produksjon i 2017. In Arnesen, F. (ed.).

WindSim. (2018). Available at: http://windsim.com/.

Appendix A: Wake influence study

The figures below provide a good visualization and understanding of the wake development of the Larsen (upper) and Jensen (lower) wake model over the wind farm with westerly wind direction of 285°. The cone representing the met mast location.

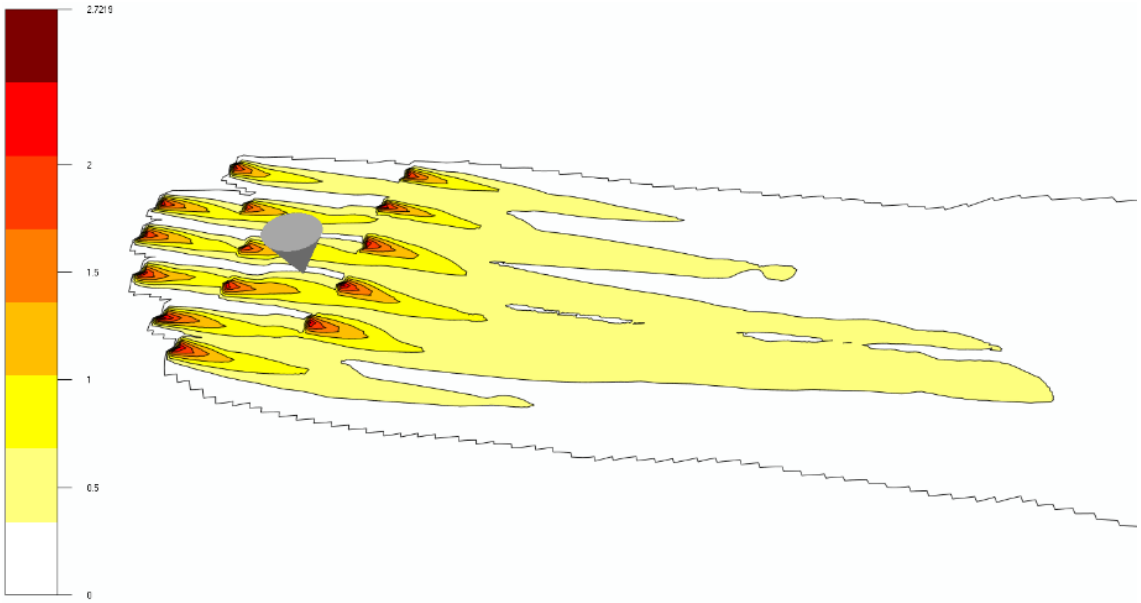

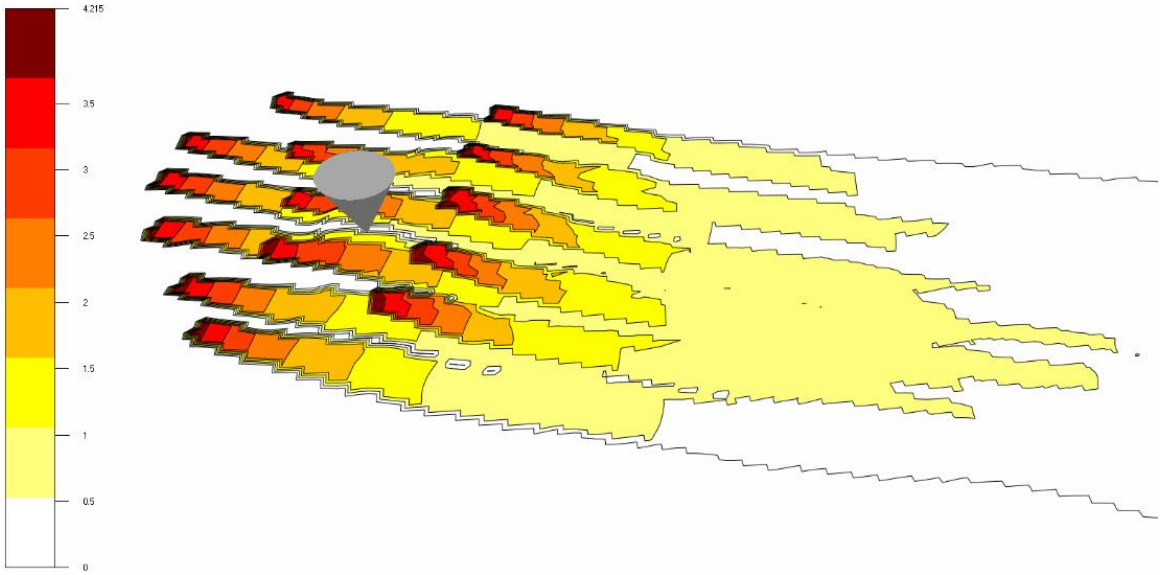

Appendix B: CFD simulations of ACD model

Residuals (left) and spot values (right) for the ACD model of sector 270 for both single and multiple wake cases. Starting with Case #1 ending with Case #7.

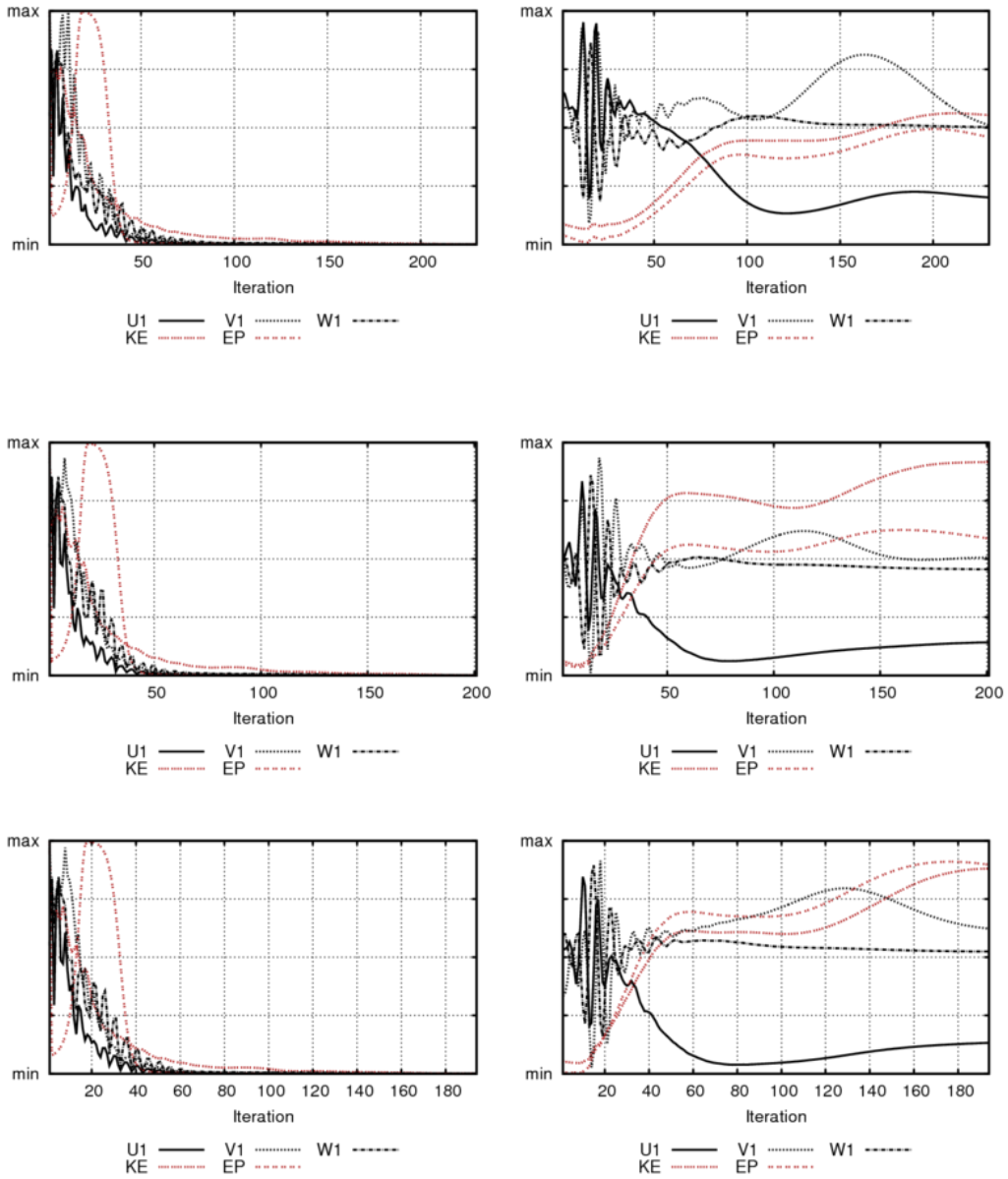

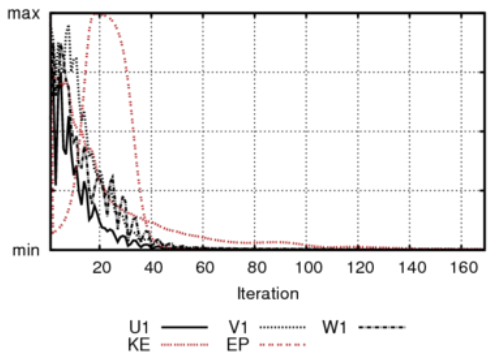
max
min
20 40 60 80 100 120 140 160
Iteration
U1 V1 W1
KE EP

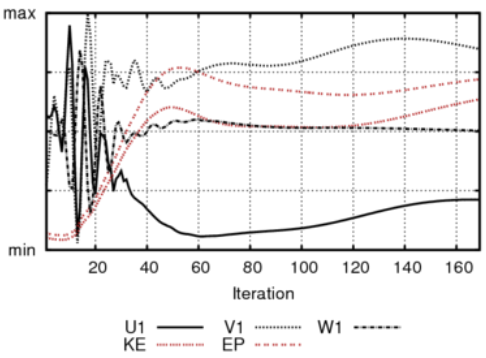
max
min
20 40 60 80 100 120 140 160
Iteration
U1 V1 W1
KE EP

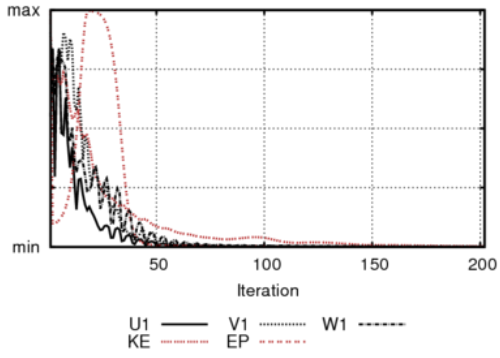
max
min
50 100 150 200
Iteration
U1 V1 W1
KE EP

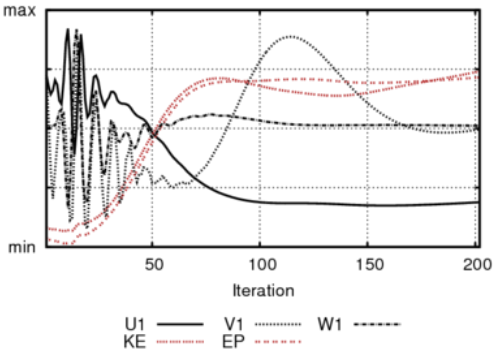
max
min
50 100 150 200
Iteration
U1 V1 W1
KE EP

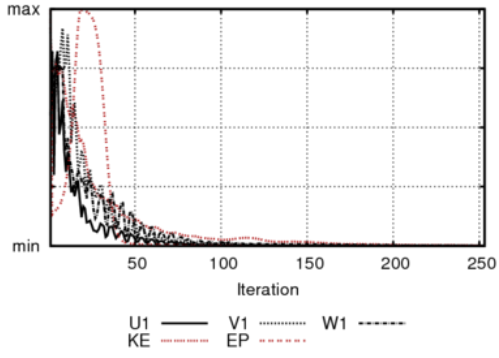
max
min
50 100 150 200 250
Iteration
U1 V1 W1
KE EP

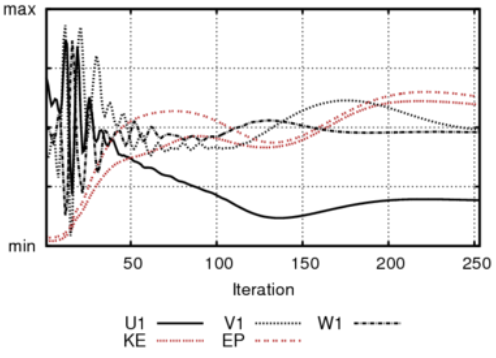
max
min
50 100 150 200 250
Iteration
U1 V1 W1
KE EP

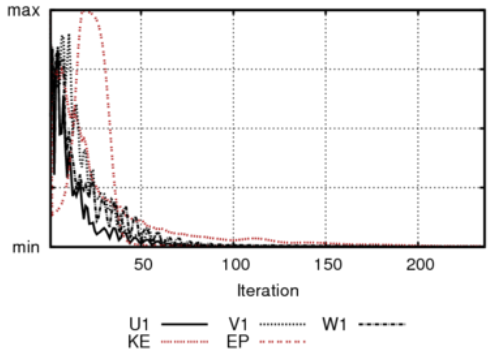
max
min
50 100 150 200
Iteration
U1 V1 W1
KE EP

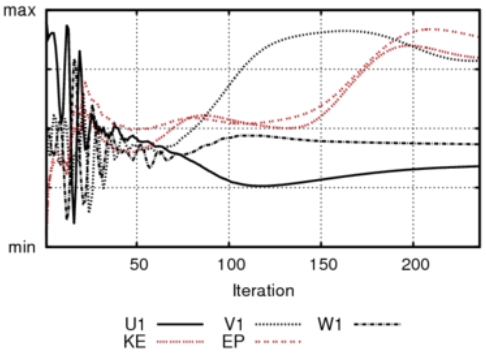
max
min
50 100 150 200
Iteration
U1 V1 W1
KE EP

Appendix C: CFD simulations of analytical model

Residuals (left) and spot values (right) for the analytical wake models of sector 270 for both single and multiple wake cases. Starting with Case #1 ending with Case #7.

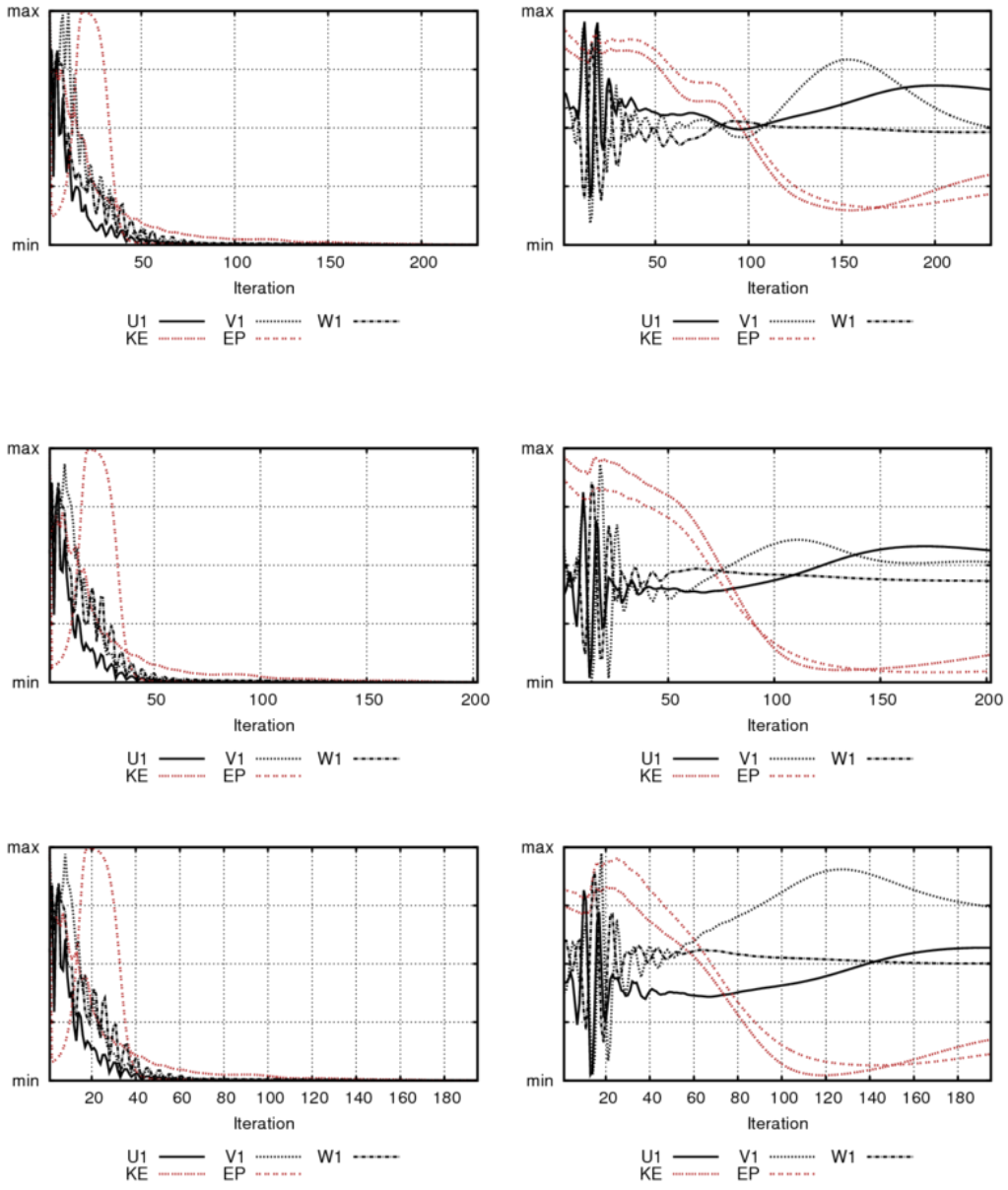

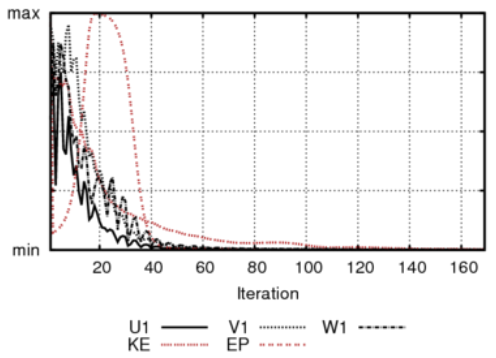
max
min
20 40 60 80 100 120 140 160
Iteration
U1 V1 W1
KE EP

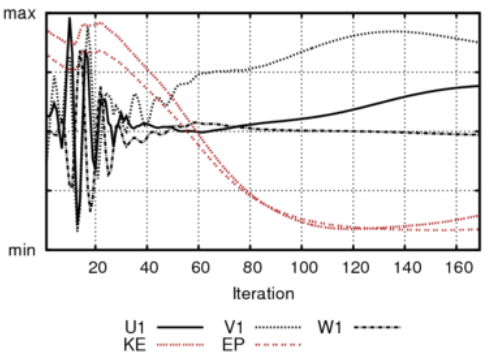
max
min
20 40 60 80 100 120 140 160
Iteration
U1 V1 W1
KE EP

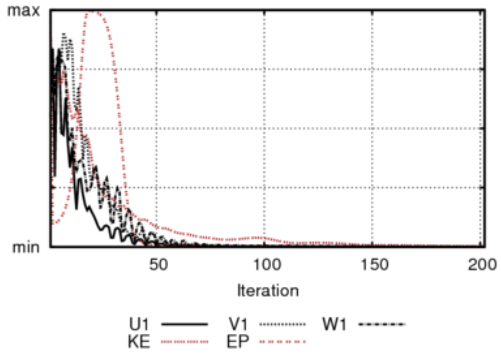
max
min
50 100 150 200
Iteration
U1 V1 W1
KE EP

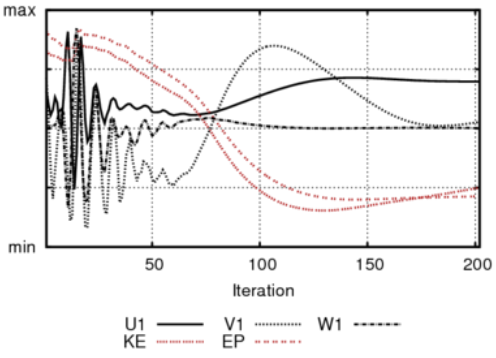
max
min
50 100 150 200
Iteration
U1 V1 W1
KE EP

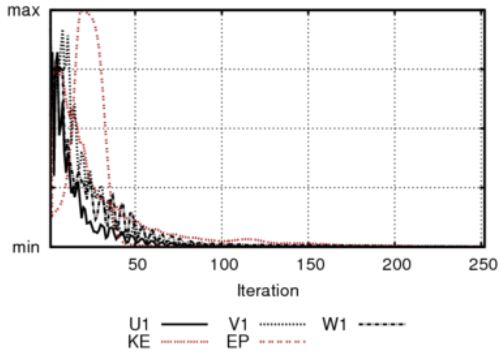
max
min
50 100 150 200 250
Iteration
U1 V1 W1
KE EP

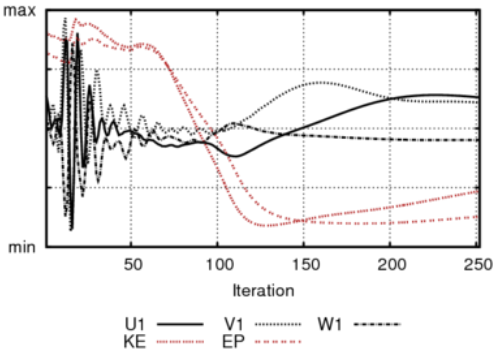
max
min
50 100 150 200 250
Iteration
U1 V1 W1
KE EP

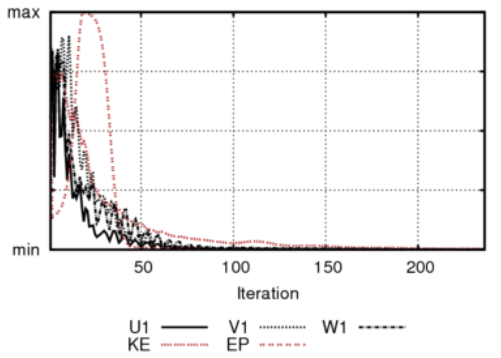
max
min
50 100 150 200
Iteration
U1 V1 W1
KE EP

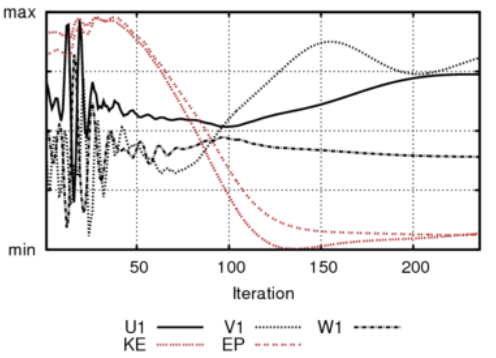
max
min
50 100 150 200
Iteration
U1 V1 W1
KE EP

Appendix D: Wind speeds at 80 m height

Visualization of wake Case #1 and Case #6 performed in WindSim using the ACD and analytical models at 80 m height and wind direction of 274.2° and 273.64° respectively. The cone represents the turbine locations. Terrain heights are also represented for the two selected cases.

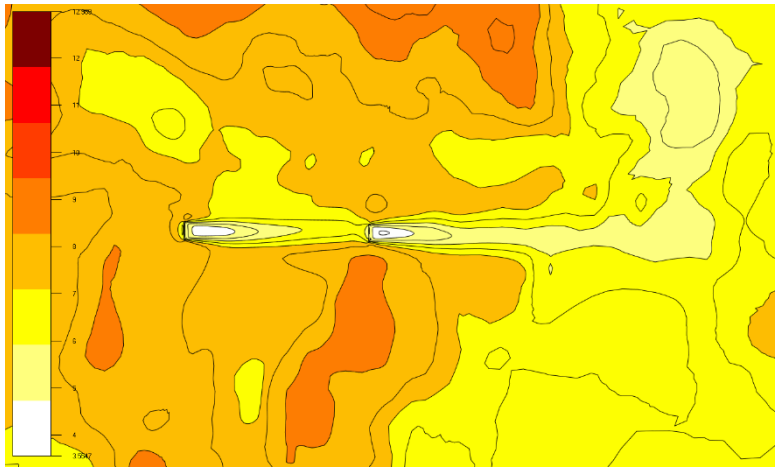

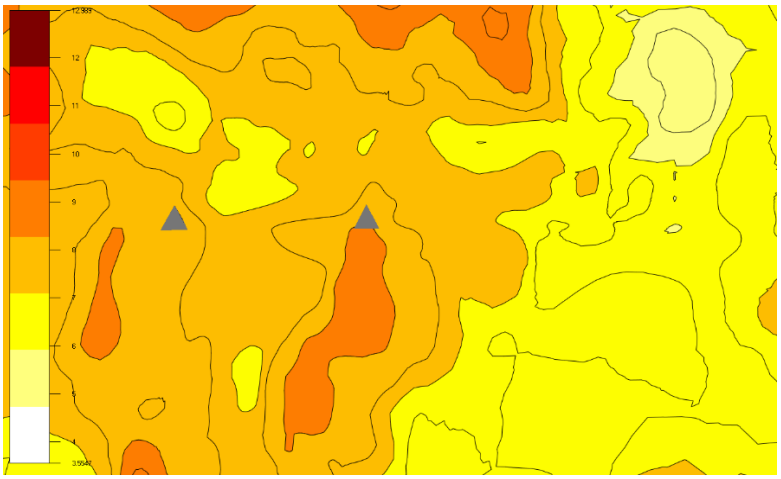

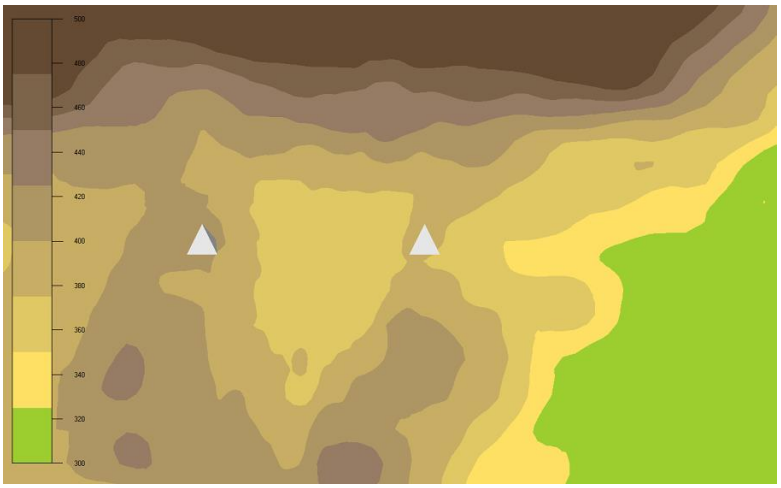

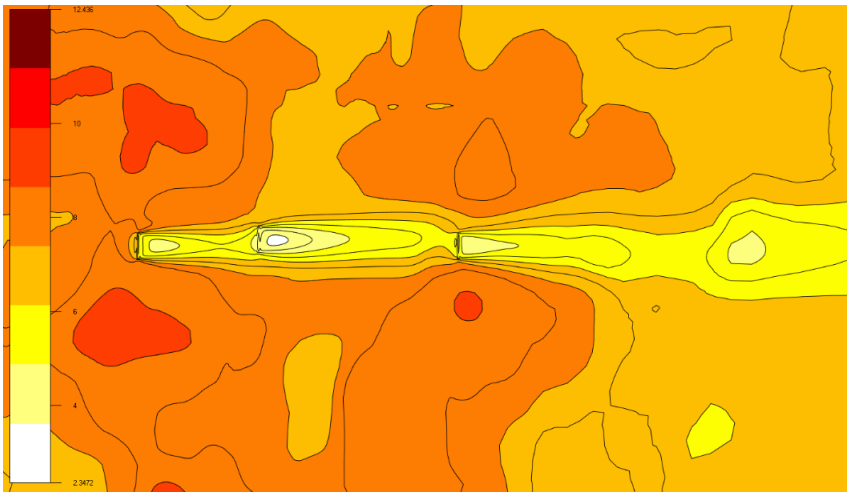
12.435
10
8
6
4
2.3472

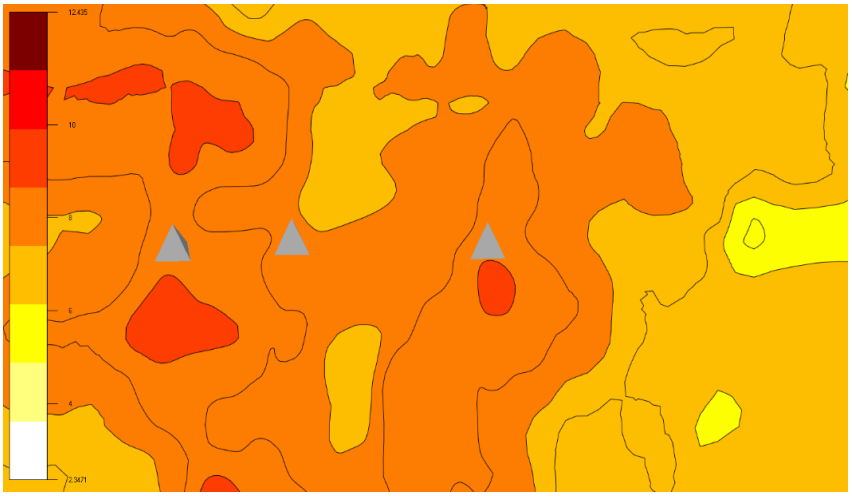
12.435
10
8
6
4
2.3471

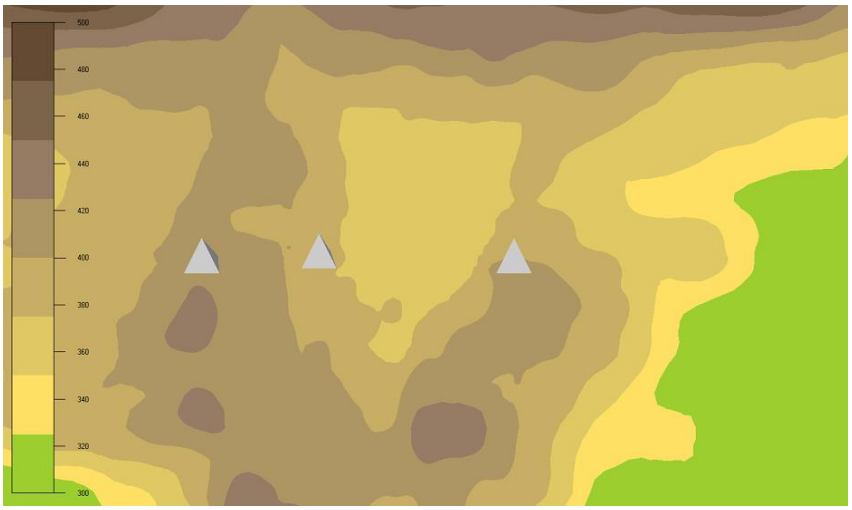
500
480
460
440
420
400
380
360
340
320
300

Appendix E: Wake expansion of the ACD, Jensen and Larsen wake model

Appendix E provides a visual representation of the wake expansion for the ACD model, Jensen and Larsen model for single wake case #1 performed in WindSim.

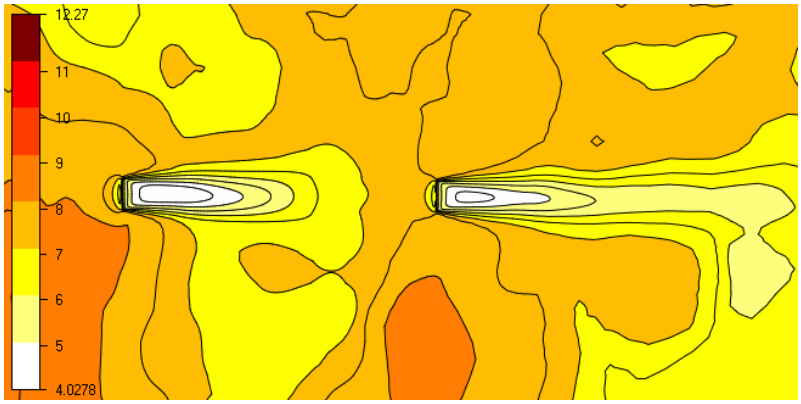

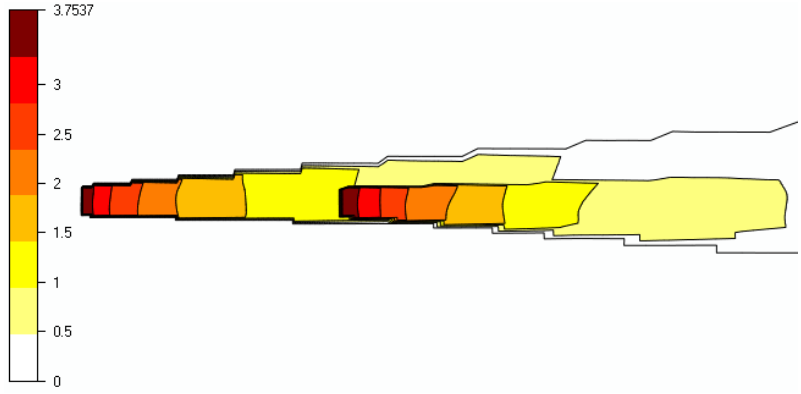

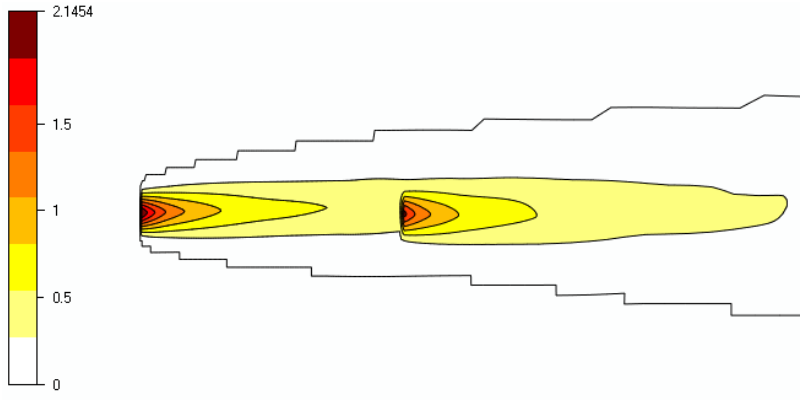

Norges miljø- og biovitenskapelige universitet
Noregs miljø- og biovitskapelege universitet
Norwegian University of Life Sciences

Postboks 5003
NO-1432 Ås
Norway